Journal of Computational Physics 229 (2010) 1238–1259

Contents lists available at ScienceDirect

Journal of Computational Physics

journal homepage: www.elsevier.com/locate/jcp

Local discontinuous Galerkin methods for the generalized Zakharov system

Yinhua Xia [a], Yan Xu [b,1], Chi-Wang Shu [a,*,2]

[a] Division of Applied Mathematics, Brown University, Providence, RI 02912, USA
[b] Department of Mathematics, University of Science and Technology of China, Hefei, Anhui 230026, PR China

ARTICLE INFO

Article history:
Received 11 February 2009
Received in revised form 10 October 2009
Accepted 14 October 2009
Available online 22 October 2009

MSC:
65M60
35K55

Keywords:
Generalized Zakharov system
Local discontinuous Galerkin methods
Energy conservation

ABSTRACT

In this paper we develop a local discontinuous Galerkin (LDG) method for the generalized Zakharov system. Two energy conservations of the LDG scheme are proved for the generalized Zakharov system. Numerical experiments for the Zakharov system are presented to illustrate the accuracy and capability of the methods, including accuracy tests, plane waves, soliton–soliton collisions of the standard and generalized Zakharov system and a two-dimensional problem.

1. Introduction

The goal of this paper is to develop a local discontinuous Galerkin (LDG) method for the generalized Zakharov system:

$$iE_t + \Delta E - Nf(|E|^2)E + g(|E|^2)E = 0,$$
$$\epsilon^2 N_{tt} - \Delta(N + F(|E|^2)) = 0,$$

which is originally introduced to describe the Langmuir turbulence in a plasma. Here, the complex function E represents the slowly varying envelope of a high-frequency plasma field, the real function N represents the deviation of ion density from its equilibrium value (an acoustic wave), ϵ is a parameter inversely proportional to the acoustic speed, and f,g,F are all given real functions. The Zakharov system is a general model governing the interaction between dispersive and non-dispersive (acoustic) waves. It has found a number of applications in various physical problems, such as in the theory of molecular chains, hydrodynamics and so on.

The generalized Zakharov system covers many generalizations of the Zakharov system in various physical applications. When $\epsilon = 1, f(|E|^2) = 1,\ g(|E|^2) = 0$ and $F(|E|^2) = |E|^2$, the system reduces to the original form of the standard Zakharov system

* Corresponding author. Tel.: +1 401 863 2549; fax: +1 401 863 1355.
E-mail addresses: yxia@dam.brown.edu (Y. Xia), yxu@ustc.edu.cn (Y. Xu), shu@dam.brown.edu (C.-W. Shu).
[1] Research supported by NSFC Grant No. 10601055, FANEDD, FANEDD of CAS and SRF for ROCS SEM.
[2] Research supported by NSF Grant No. DMS-0809086 and ARO grant W911NF-08-1-0520.

0021-9991/$ - see front matter © 2009 Elsevier Inc. All rights reserved.
doi:10.1016/j.jcp.2009.10.029

$$iE_t + \Delta E - NE = 0,$$
$$N_{tt} - \Delta(N + |E|^2) = 0,$$

which was first proposed by Zakharov [34] in 1972. In the singular limit $\epsilon \to 0$ (infinite acoustic speed, the subsonic limit), the system reduces to the nonlinear Schrödinger equation (NLS):

$$iE_t + \Delta E + F(|E|^2)f(|E|^2)E + g(|E|^2)E = 0.$$

Many numerical methods have been developed for the Zakharov system in the last two decades. In 1983, Payne et al. [21] proposed a Fourier spectral method for the one-dimensional standard Zakharov system. Only two-thirds of the Fourier components have been used in their scheme to suppress the aliasing errors. In 1992, Glassey [12,13] developed an energy-preserving implicit finite difference scheme for the Zakharov system in one dimension, and proved its convergence. Chang et al. [5,4] presented implicit and semi-implicit conservative difference schemes for the one-dimensional generalized Zakharov system. They also proved the second order convergence of their method. Recently, time-splitting spectral methods have been proposed by Bao et al. [3,2] and Jin et al. [17,18] to solve the generalized Zakharov system and vector Zakharov system for multi-component plasmas.

The local discontinuous Galerkin (LDG) method is an extension of the discontinuous Galerkin (DG) method aimed at solving partial differential equations (PDEs) containing higher than first order spatial derivatives. The DG method is a class of finite element methods, using discontinuous, piecewise polynomials as the solution and the test space. It was first designed as a method for solving hyperbolic conservation laws containing only first order spatial derivatives, e.g. Reed and Hill [22] for solving linear equations, and Cockburn et al. [8,7,6,9] for solving nonlinear equations. It is difficult to apply the DG method directly to the equations with higher order derivatives. The idea of the LDG method is to rewrite the equations with higher order derivatives into a first order system, then apply the DG method on the system. The design of the numerical fluxes is the key ingredient to ensure stability.

The first LDG method was constructed by Cockburn and Shu in [10] for solving nonlinear convection diffusion equations containing second order spatial derivatives. Their work was motivated by the successful numerical experiments of Bassi and Rebay [1] for the compressible Navier–Stokes equations. Yan and Shu developed a LDG method for a general KdV type equation (containing third order spatial derivatives) in [32], and they generalized the LDG method to PDEs with fourth and fifth order spatial derivatives in [33]. Levy et al. [19] developed LDG methods for nonlinear dispersive equations that have compactly supported traveling wave solutions, the so-called "compactons". More recently, Xu and Shu [27–31] further developed the LDG method to solve many nonlinear wave equations including the general KdV–Burgers type equations, the general fifth order KdV type equations, the fully nonlinear $K(n, n, n)$ equations, the generalized nonlinear Schrödinger equations, the coupled nonlinear Schrödinger equations, the Kuramoto–Sivashinsky equations, the Ito-type coupled KdV equations, the Kadomtsev–Petviashvili equation, the Zakharov–Kuznetsov equation and the Camassa–Holm equation. Xia et al. [25,26] developed the LDG method to solve the Allen–Cahn and Cahn–Hilliard type equations. Recently, a LDG method for solving the porous medium equation is designed in [35]. A common feature of these LDG methods is that stability can be proved for quite general nonlinear cases. DG and LDG methods also have several attractive properties, such as their flexibility for arbitrary *hp* adaptivity and their excellent parallel efficiency.

This paper is organized as follows. In Section 2, we present and analyze the LDG method for the generalized Zakharov system. In Section 2.1, we review the Zakharov system and its conservation laws. In Section 2.2 we develop the LDG scheme for the Zakharov system and prove the conservation properties of the LDG scheme. In Section 3, we perform numerical experiments to show the accuracy and capability of the scheme, including accuracy tests, plane waves, soliton–soliton collisions of the standard and generalized Zakharov systems and two-dimensional problems. Concluding remarks are given in Section 4.

2. The LDG method for the generalized Zakharov system

In this section we will develop the LDG for the generalized Zakharov system.

2.1. Conservation laws of the generalized Zakharov system

We restrict ourselves to the bounded domain $\Omega \in \mathbb{R}^d$ with periodic or Dirichlet boundary conditions. Consider the following initial boundary value problem of the generalized Zakharov system:

$$iE_t + \Delta E - Nf(|E|^2)E + g(|E|^2)E = 0, \quad \boldsymbol{x} \in \Omega,\ t > 0, \tag{2.1a}$$
$$\epsilon^2 N_{tt} - \Delta(N + F(|E|^2)) = 0, \quad \boldsymbol{x} \in \Omega,\ t > 0, \tag{2.1b}$$

with initial conditions and the compatibility condition

$$E(\boldsymbol{x}, 0) = E_0(\boldsymbol{x}), \quad N(\boldsymbol{x}, 0) = N_0(\boldsymbol{x}, 0), \quad N_t(\boldsymbol{x}, 0) = N_1(\boldsymbol{x}), \quad \int_\Omega N_1(\boldsymbol{x})d\boldsymbol{x} = 0, \quad \boldsymbol{x} \in \Omega, \tag{2.2}$$

and periodic boundary conditions for all variables or the Dirichlet boundary conditions

$$E(\boldsymbol{x},t)=0,\quad N(\boldsymbol{x},t)=0,\quad \boldsymbol{x}\in\partial\Omega. \tag{2.3}$$

The wave energy $D=\int_\Omega |E|^2$ of the generalized Zakharov system is conserved [34]:

$$\frac{d}{dt}D=\frac{d}{dt}\int_\Omega |E|^2 d\boldsymbol{x}=0. \tag{2.4}$$

Introducing a new unknown function $\boldsymbol{V}=(V_1,\ldots,V_d)$,

$$\epsilon N_t+\nabla\cdot\boldsymbol{V}=0, \tag{2.5}$$

it is easy to verify that the Hamiltonian H of the generalized Zakharov system is also conserved [11],

$$\frac{d}{dt}H=\frac{d}{dt}\int_\Omega\left(|\nabla E|^2+\frac{1}{2}\left(\boldsymbol{V}\cdot\boldsymbol{V}+N^2\right)+NF(|E|^2)+G(|E|^2)\right)d\boldsymbol{x}=0, \tag{2.6}$$

if $F(s)=\int^s f(\tau)d\tau, G(s)=\int^s g(\tau)d\tau$.

Remark 2.1. When $f(|E|^2)=1, F(|E|^2)=|E|^2$ and $g(|E|^2)=0$, the generalized Zakharov system becomes the standard Zakharov system

$$iE_t+\Delta E-NE=0, \tag{2.7a}$$
$$\epsilon^2 N_{tt}-\Delta(N+|E|^2)=0. \tag{2.7b}$$

The extra conserved quantity of the standard Zakharov system (2.7) is the momentum [11]

$$\boldsymbol{P}=\int_\Omega\left(\frac{i}{2}(E\nabla E^*-E^*\nabla E)+\epsilon N\boldsymbol{V}\right)d\boldsymbol{x}. \tag{2.8}$$

Remark 2.2. When $f(|E|^2)=-2, F(|E|^2)=-v|E|^2$ and $g(|E|^2)=2\lambda|E|^2$, the generalized Zakharov system becomes

$$iE_t+\Delta E+2NE+2\lambda|E|^2E=0, \tag{2.9a}$$
$$\epsilon^2 N_{tt}-\Delta(N-v|E|^2)=0, \tag{2.9b}$$

which is introduced in [14] and simulated in [3,17,18]. For this type of generalized Zakharov system, the Hamiltonian H is no longer a conserved quantity when $v\neq -2$.

Remark 2.3. One can also add a damping term in the Schrödinger equation and a dissipative term in the wave equation [3,14,15]

$$iE_t+\Delta E-Nf(|E|^2)E+g(|E|^2)E+i\gamma E=0,\quad \gamma>0, \tag{2.10a}$$
$$\epsilon^2 N_{tt}-\Delta(N+F(|E|^2))=\mu(\Delta N)_t,\quad \mu>0, \tag{2.10b}$$

in which $D(t)=e^{-2\gamma t}D(0)$.

2.2. The LDG method for the generalized Zakharov system

In this section, we develop the LDG method for the generalized Zakharov system (2.1).

Let $\mathcal{T}_h$ denote a tessellation of Ω with shape-regular elements K. Let Γ denote the union of the boundary faces of elements $K\in\mathcal{T}_h$, i.e. $\Gamma=\cup_{K\in\mathcal{T}_h}\partial K$, and $\Gamma_0=\Gamma\setminus\partial\Omega$. In order to describe the flux functions we need to introduce some notations. Let e be a face shared by the "left" and "right" elements K_L and K_R. For our purpose "left" and "right" can be uniquely defined for each face according to any fixed rule, see, e.g. [32] for more details of such a definition. Define the normal vectors $\boldsymbol{v}_L$ and $\boldsymbol{v}_R$ on e pointing exterior to K_L and K_R, respectively. If ψ is a function on K_L and K_R, but possibly discontinuous across e, let ψ_L denote $(\psi|_{K_L})|_e$ and ψ_R denote $(\psi|_{K_R})|_e$, the left and right trace, respectively.

Let ${}_r\mathcal{P}^k(K)$ and ${}_c\mathcal{P}^k(K)$ be the space of real and complex polynomials of degree at most $k\geqslant 0$ on $K\in\mathcal{T}_h$, respectively. The finite element spaces are denoted by

$${}_rS_h=\{\varphi:\varphi|_K\in{}_r\mathcal{P}^k(K),\forall K\in\mathcal{T}_h\},$$
$${}_r\Sigma_h^d=\left\{\Phi=(\phi_1,\ldots,\phi_d)^T:\phi_l|_K\in{}_r\mathcal{P}^k(K),l=1,\ldots,d,\forall K\in\mathcal{T}_h\right\},$$
$${}_cS_h=\{\varphi:\varphi|_K\in{}_c\mathcal{P}^k(K),\forall K\in\mathcal{T}_h\},$$
$${}_c\Sigma_h^d=\left\{\Phi=(\phi_1,\ldots,\phi_d)^T:\phi_l|_K\in{}_c\mathcal{P}^k(K),l=1,\ldots d,\forall K\in\mathcal{T}_h\right\}.$$

Note that functions in ${}_rS_h$, ${}_r\Sigma_h^d$, ${}_cS_h$ and ${}_c\Sigma_h^d$ are allowed to be completely discontinuous across element interfaces.

To construct the LDG method, firstly we rewrite the generalized Zakharov system (2.1) as a system containing only first order derivatives:

$$\boldsymbol{M} = \nabla E, \tag{2.11a}$$

$$iE_t + \nabla\cdot\boldsymbol{M} - Nf(|E|^2)E + g(|E|^2)E = 0, \tag{2.11b}$$

$$\epsilon N_t + \nabla\cdot\boldsymbol{V} = 0, \tag{2.11c}$$

$$\epsilon\boldsymbol{V}_t + \nabla(N+S) = 0, \tag{2.11d}$$

$$S = F(|E|^2). \tag{2.11e}$$

To simplify the notation, we still use $\boldsymbol{M}, E, N, \boldsymbol{V}$ and S to denote the numerical solution. The LDG scheme to solve the generalized Zakharov system (2.11e) is as follows: find $E \in {}_cS_h, N,\ S \in {}_rS_h$ and $\boldsymbol{M} \in {}_c\Sigma_h^d,\ \boldsymbol{V} \in {}_r\Sigma_h^d$ such that, for all test functions $u \in {}_cS_h, v,\ r \in {}_rS_h$ and $\boldsymbol{Q} \in {}_c\Sigma_h^d,\ \boldsymbol{W} \in {}_r\Sigma_h^d$

$$\int_K \boldsymbol{M}\cdot\boldsymbol{Q} = \int_{\partial K} \widehat{E}\boldsymbol{Q}\cdot v ds - \int_K E\nabla\cdot\boldsymbol{Q} dK, \tag{2.12a}$$

$$\int_K iE_t u dK + \int_{\partial K} \widehat{\boldsymbol{M}}\cdot v u ds - \int_K \boldsymbol{M}\cdot\nabla u dK + \int_K (-Nf(|E|^2)E + g(|E|^2)E)u dK = 0, \tag{2.12b}$$

$$\int_K \epsilon N_t v dK + \int_{\partial K} \widehat{\boldsymbol{V}}\cdot v v ds - \int_K \boldsymbol{V}\cdot\nabla v dK = 0, \tag{2.12c}$$

$$\int_K \epsilon\boldsymbol{V}_t\cdot\boldsymbol{W} dK + \int_{\partial K} \widehat{(N+S)}\boldsymbol{W}\cdot v ds - \int_K (N+S)\nabla\cdot\boldsymbol{W} dK = 0, \tag{2.12d}$$

$$\int_K S r dK = \int_K F(|E|^2) r dK. \tag{2.12e}$$

The "hat" terms in (2.12a)–(2.12e) in the cell boundary terms from integration by parts are the so-called "numerical fluxes", which are functions defined on the edges and should be designed based on different guiding principles for different PDEs to ensure stability and local solvability of the intermediate variables $\boldsymbol{M}, S$.

In the following procedure of proving the two conservation laws (2.4) and (2.6), it turns out that we can take the simple choices such as

$$\widehat{\boldsymbol{M}}|_e = \boldsymbol{M}_L, \quad \widehat{E}|_e = E_R, \quad \widehat{\boldsymbol{V}}|_e = \boldsymbol{V}_L, \quad \widehat{N+S}|_e = (N+S)_R. \tag{2.13}$$

We remark that the choice for the fluxes (2.13) is not unique. Considering the compactness of the stencil and optimal accuracy, the crucial part is taking $\widehat{\boldsymbol{M}}$ and $\widehat{E}$ from opposite sides and $\widehat{\boldsymbol{V}}$ and $\widehat{N+S}$ from opposite sides.

Proposition 2.1 (Conservation laws). *The solution to the LDG scheme (2.12) and (2.13) satisfies the conservation of the wave energy*

$$\frac{d}{dt}\int_\Omega |E|^2 d\boldsymbol{x} = 0,$$

and if $F(s) = \int^s f(\tau)d\tau$, the scheme also satisfies

$$\frac{d}{dt}\int_\Omega \left(|\boldsymbol{M}|^2 + \frac{1}{2}(\boldsymbol{V}\cdot\boldsymbol{V} + N^2) + NF(|E|^2) + G(|E|^2)\right) d\boldsymbol{x} = 0,$$

where $G(s) = -\int^s g(\tau)d\tau$.

Proof. Let E^* represent the conjugate of E. Choosing the test function $u = E^*$ in (2.12b), we obtain

$$\int_K iE_t E^* dK + \int_{\partial K} \widehat{\boldsymbol{M}}\cdot v E^* ds - \int_K \boldsymbol{M}\cdot\nabla E^* dK + \int_K \left(-Nf(|E|^2)E + g(|E|^2)E\right)E^* dK = 0, \tag{2.14}$$

and taking the conjugate of the Eq. (2.14), we get

$$\int_K -iE_t^* E dK + \int_{\partial K} \widehat{\boldsymbol{M}}^*\cdot v E ds - \int_K \boldsymbol{M}^*\cdot\nabla E dK + \int_K \left(-Nf(|E|^2)E^* + g(|E|^2)E^*\right)E dK = 0. \tag{2.15}$$

Similarly, setting the test function $\boldsymbol{Q} = \boldsymbol{M}^*$ in (2.12a) and then taking the conjugate, we have

$$\int_K \boldsymbol{M}\cdot\boldsymbol{M}^* = \int_{\partial K} \widehat{E}\boldsymbol{M}^*\cdot v ds - \int_K E\nabla\cdot\boldsymbol{M}^* dK, \tag{2.16}$$

$$\int_K \boldsymbol{M}^*\cdot\boldsymbol{M} = \int_{\partial K} \widehat{E}^*\boldsymbol{M}\cdot v ds - \int_K E^*\nabla\cdot\boldsymbol{M} dK. \tag{2.17}$$

If we add (2.14) and (2.16), and subtract from it the sum of (2.15) and (2.17), we get

$$\int_K i(EE^*)_t dK + \int_{\partial K} \widehat{\boldsymbol{M}} \cdot \boldsymbol{v} E^* ds + \int_{\partial K} \widehat{E}^* \boldsymbol{M} \cdot \boldsymbol{v} ds - \int_K \nabla \cdot (E^* \boldsymbol{M}) dK - \left(\int_{\partial K} \widehat{\boldsymbol{M}^*} \cdot \boldsymbol{v} E ds + \int_{\partial K} \widehat{E} \boldsymbol{M}^* \cdot \boldsymbol{v} ds - \int_K \nabla \cdot (E \boldsymbol{M}^*) dK \right) = 0. \tag{2.18}$$

Summing up the Eq. (2.18) over K, and noticing that the fluxes $\widehat{\boldsymbol{M}}$ and $\widehat{E}$ are from opposite sides of ∂K as well as the boundary conditions, we obtain

$$\frac{d}{dt} \int_\Omega |E|^2 d\boldsymbol{x} = 0.$$

For the second conservation law, we take the time derivative of Eq. (2.12a) and choose the test function $\boldsymbol{Q} = \boldsymbol{M}^*$ to obtain

$$\int_K \boldsymbol{M}_t \cdot \boldsymbol{M}^* = \int_{\partial K} \widehat{E}_t \boldsymbol{M}^* \cdot \boldsymbol{v} ds - \int_K E_t \nabla \cdot \boldsymbol{M}^* dK, \tag{2.19}$$

and its conjugate

$$\int_K \boldsymbol{M}_t^* \cdot \boldsymbol{M} = \int_{\partial K} \widehat{E_t^*} \boldsymbol{M} \cdot \boldsymbol{v} ds - \int_K E_t^* \nabla \cdot \boldsymbol{M} dK. \tag{2.20}$$

In (2.12b), we choose the test function $u = E_t^*$ to obtain

$$\int_K i E_t E_t^* dK + \int_{\partial K} \widehat{\boldsymbol{M}} \cdot \boldsymbol{v} E_t^* ds - \int_K \boldsymbol{M} \cdot \nabla E_t^* dK + \int_K \left(-Nf(|E|^2)E + g(|E|^2)E \right) E_t^* dK = 0, \tag{2.21}$$

and its conjugate

$$\int_K -i E_t^* E_t dK + \int_{\partial K} \widehat{\boldsymbol{M}^*} \cdot \boldsymbol{v} E_t ds - \int_K \boldsymbol{M}^* \cdot \nabla E_t dK + \int_K \left(-Nf(|E|^2)E^* + g(|E|^2)E^* \right) E_t dK = 0. \tag{2.22}$$

In (2.12c), (2.12d) and (2.12e), we set the test function $v = N + S, \boldsymbol{W} = \boldsymbol{V}$ and $r = N_t$, respectively to obtain

$$\int_K \epsilon N_t (N+S) dK + \int_{\partial K} \widehat{\boldsymbol{V}} \cdot \boldsymbol{v} (N+S) ds - \int_K \boldsymbol{V} \cdot \nabla (N+S) dK = 0, \tag{2.23}$$

$$\int_K \epsilon \boldsymbol{V}_t \cdot \boldsymbol{V} dK + \int_{\partial K} \widehat{(N+S)} \boldsymbol{V} \cdot \boldsymbol{v} ds - \int_K (N+S) \nabla \cdot \boldsymbol{V} dK = 0, \tag{2.24}$$

$$\int_K S N_t dK = \int_K F(|E|^2) N_t dK. \tag{2.25}$$

Table 3.1
Accuracy test in Example 3.1 for $\epsilon = 1$ at time $t = 2$, with piecewise P^3 and P^4 polynomial bases.

	h	P^3				P^4			
		L^∞ error	Order	L^2 error	Order	L^∞ error	Order	L^2 error	Order
$Re(E)$	2	1.61E−02	–	1.77E−02	–	3.22E−03	–	3.25E−03	–
	1	7.27E−04	4.47	8.44E−04	4.39	9.99E−05	5.02	1.58E−04	4.36
	1/2	1.01E−04	2.85	7.21E−05	3.55	4.45E−06	4.49	4.66E−06	5.08
	1/4	6.78E−06	3.90	4.36E−06	4.05	1.23E−07	5.17	1.22E−07	5.26
	1/8	4.32E−06	3.97	2.72E−07	4.00	4.48E−09	4.78	3.57E−09	5.09
$Im(E)$	2	2.13E−02	–	2.53E−03	–	3.16E−03	–	2.90E−03	–
	1	9.82E−04	4.43	8.28E−04	4.93	1.39E−04	4.50	2.08E−04	3.80
	1/2	1.34E−04	2.87	9.35E−05	3.15	5.74E−06	4.60	5.86E−06	5.15
	1/4	9.94E−06	3.75	6.02E−06	3.96	1.94E−07	4.89	1.76E−07	5.06
	1/8	6.56E−07	3.92	3.77E−07	4.00	6.08E−09	4.99	5.01E−09	5.13
N	2	8.58E−02	–	9.32E−02	–	5.46E−03	–	7.26E−03	–
	1	1.88E−03	5.51	1.95E−03	5.58	9.40E−04	2.54	5.24E−04	3.79
	1/2	4.72E−04	1.99	3.45E−04	2.50	1.39E−05	6.08	1.13E−05	5.54
	1/4	3.39E−05	3.80	2.15E−05	4.00	7.07E−07	4.30	4.81E−07	4.55
	1/8	2.48E−06	3.77	1.40E−06	3.94	1.76E−08	5.32	1.05E−08	5.52

Let (2.19) + (2.20) − (2.21) − (2.22)+[(2.23) + (2.24)]/ϵ − (2.25), we have

$$\begin{aligned}
&\frac{d}{dt}\int_K \left(\boldsymbol{M}\boldsymbol{M}^* + \frac{1}{2}(\boldsymbol{V}\cdot\boldsymbol{V} + N^2) + NF(|E|^2) + G(|E|^2)\right)dK \\
&= \int_{\partial K} \widehat{E}_t \boldsymbol{M}^* \cdot \boldsymbol{v} ds + \int_{\partial K} \widehat{\boldsymbol{M}^*} \cdot \boldsymbol{v} E_t ds - \int_K \nabla\cdot(\boldsymbol{M}^* E_t) dK + \int_{\partial K} \widehat{E_t^*}\boldsymbol{M}\cdot\boldsymbol{v} ds + \int_{\partial K} \widehat{\boldsymbol{M}}\cdot\boldsymbol{v} E_t^* ds \\
&\quad - \int_K \nabla\cdot(\boldsymbol{M}E_t^*) dK - \frac{1}{\epsilon}\left(\int_{\partial K} \widehat{\boldsymbol{V}}\cdot\boldsymbol{v}(N+S) ds + \int_{\partial K} \widehat{(N+S)}\boldsymbol{V}\cdot\boldsymbol{v} ds - \int_K \nabla\cdot((N+S)\boldsymbol{V}) dK\right).
\end{aligned} \tag{2.26}$$

Finally, summing up Eq. (2.26) over K and noticing the fluxes $\widehat{(N+S)}$ and $\widehat{\boldsymbol{V}}$ are from the opposite sides of ∂K as well as the boundary conditions, we obtain

$$\frac{d}{dt}\int_\Omega \left(|\boldsymbol{M}|^2 + \frac{1}{2}(\boldsymbol{V}\cdot\boldsymbol{V} + N^2) + NF(|E|^2) + G(|E|^2)\right)d\boldsymbol{x} = 0. \qquad \square$$

Remark 2.4. The numerical fluxes for the scheme (2.12) can also be chosen as the central numerical fluxes

$$\widehat{\boldsymbol{M}}|_e = \frac{(\boldsymbol{M}_L + \boldsymbol{M}_R)}{2}, \quad \widehat{E}|_e = \frac{(E_L + E_R)}{2}, \quad \widehat{\boldsymbol{V}}|_e = \frac{(\boldsymbol{V}_L + \boldsymbol{V}_R)}{2}, \quad \widehat{N+S}|_e = \frac{((N+S)_L + (N+S)_R)}{2},$$

Table 3.2
Accuracy test in Example 3.1 for $\epsilon = 10^{-4}$ at time $t = 2$, with piecewise P^3 and P^4 polynomial bases.

	h	P^3				P^4			
		L^∞ error	Order	L^2 error	Order	L^∞ error	Order	L^2 error	Order
$Re(E)$	2	2.42E−02	–	3.10E−02	–	5.63E−03	–	5.91E−03	–
	1	8.80E−04	4.78	1.22E−03	4.66	1.53E−05	5.20	2.21E−04	4.74
	1/2	1.18E−04	2.90	9.68E−05	3.66	5.27E−06	4.86	6.35E−06	5.12
	1/4	5.34E−06	4.47	5.06E−06	4.26	1.11E−07	5.57	1.63E−07	5.28
	1/8	4.56E−07	3.55	3.75E−07	3.75	3.65E−09	4.93	4.81E−09	5.08
$Im(E)$	2	2.83E−02	–	3.64E−02	–	3.46E−02	–	4.92E−03	–
	1	1.13E−03	4.65	1.13E−03	5.00	1.94E−04	4.16	2.76E−04	4.16
	1/2	1.54E−04	2.87	1.18E−04	3.26	6.50E−06	4.90	7.48E−06	5.21
	1/4	1.30E−05	3.57	8.33E−06	3.83	2.42E−07	4.75	2.59E−07	4.85
	1/8	5.64E−07	4.53	4.07E−07	4.36	5.77E−09	5.39	6.44E−09	5.33
N	2	1.08E−01	–	1.09E−01	–	8.04E−03	–	6.92E−03	–
	1	2.01E−03	5.75	1.93E−03	5.82	5.59E−04	3.84	6.23E−04	3.47
	1/2	4.67E−04	2.11	3.58E−04	2.43	1.87E−05	4.90	1.69E−05	5.21
	1/4	4.61E−05	3.34	2.36E−05	3.92	6.25E−07	4.90	5.23E−07	5.01
	1/8	2.90E−06	3.99	1.49E−06	3.99	2.14E−08	4.87	1.65E−08	4.99

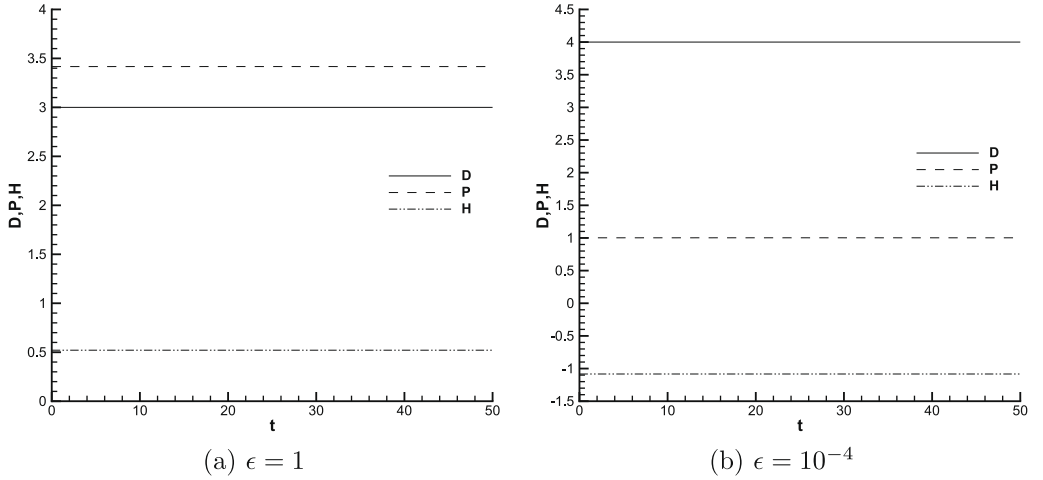

Fig. 3.1. Numerical results in Example 3.1, with piecewise P^3 polynomial basis and mesh size $h = 1$: the energies$D$, P and H: (a) $\epsilon = 1$, and (b) $\epsilon = 10^{-4}$.

which would yield a scheme which also satisfies Proposition 2.1. However, this choice gives a scheme which is less compact in the stencil and sub-optimal in the order of accuracy for odd k (i.e. the accuracy is order k rather than the expected order $k+1$ for odd k), see [10] for a discussion in the context of a dissipative equation. In our numerical test, we use the fluxes (2.13) and the optimal accuracy order can be obtained.

Remark 2.5. The LDG scheme can be applied to the generalized Zakharov system (2.10), by rewriting the system into

$$\begin{aligned}
&\boldsymbol{M} = \nabla E,\\
&iE_t + \nabla\cdot\boldsymbol{M} - Nf(|E|^2)E + g(|E|^2)E + i\gamma E = 0,\\
&\epsilon N_t + \nabla\cdot\boldsymbol{V} = 0,\\
&W + \frac{\mu}{\epsilon}\nabla\cdot\boldsymbol{V} = 0,\\
&\epsilon\boldsymbol{V}_t + \nabla(N + S + W) = 0,\\
&S = F(|E|^2).
\end{aligned}$$

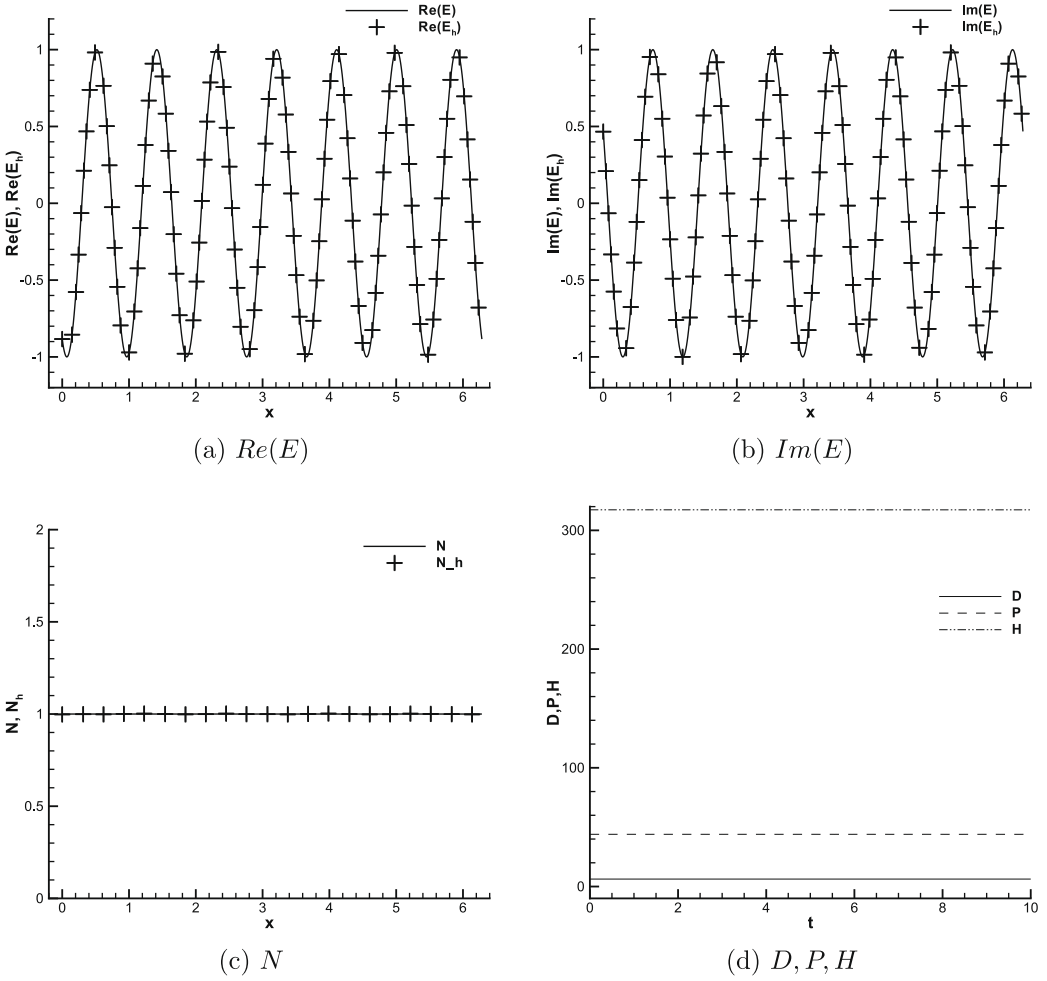

Fig. 3.2. Numerical results in Example 3.2: (a–c) Numerical solutions of $Re(E_h), Im(E_h)$ and N_h comparing with exact solutions $Re(E), Im(E)$ and N at $t = 10$; and (d) the energies D, P and H evolving with time.

Table 3.3
Parameters used in Example 3.3 of periodic soliton–soliton collisions.

Parameter set	L	E_{max}	E_{min}	v	u	N_0
A	160	1.0	1.0535E−31	0.628319	2.24323	0.0227232
B	160	0.5	1.0535E−18	0.628319	−0.27094	0.0227232
C	160	1.0	1.0535E−38	0.314159	−3.22992	0.0227232

The numerical fluxes are similar to (2.13) with $\widehat{N+S}$ replaced by $(N+\widehat{S+W})$. It is easy to verify $D(t) = e^{-2\gamma t}D(0)$ for the LDG scheme following a similar proof as that for Proposition 2.1.

3. Numerical tests

In this section, we present numerical tests of the Zakharov system with a solitary wave solution in one dimension to test the accuracy and ϵ resolution of the LDG scheme developed in Section 2. We also present numerical examples including plane-wave, soliton–soliton collisions in one dimension, as well as a two-dimensional problem of the Zakharov system to demonstrate the capability of the method. Time discretization method is the TVD Runge–Kutta method [23]. The stability constraint between the time step Δt and the mesh size h is $\Delta t = O(\min(\epsilon h, h^2))$. This is not the most efficient time discret-

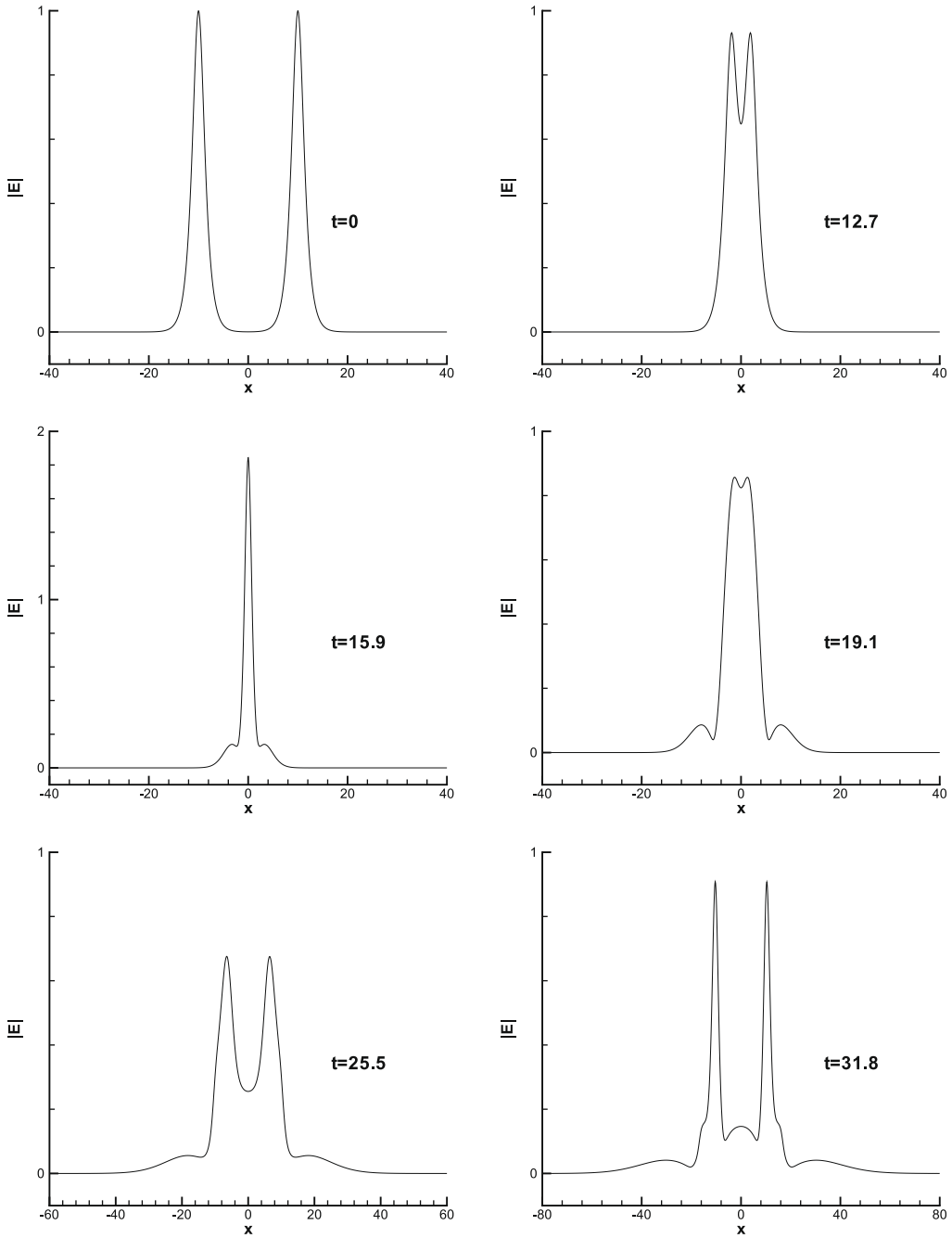

Fig. 3.3. Numerical results at different times in Example 3.3 for case I: electric field $|E|$.

ization method to the LDG scheme of the Zakharov system. Semi-implicit time discretization methods can be used to increase the efficiency [24]. However, we will not address the efficiency of time discretization in this paper. We choose the time step suitably small such that the spatial errors are dominant in the numerical results. With successive mesh refinements, we have verified that all numerical results are mesh convergent.

3.1. The one-dimensional Zakharov system

Example 3.1 (*Accuracy test*). Consider the one-dimensional standard Zakharov system

$$iE_t + E_{xx} - NE = 0, \tag{3.27a}$$

$$\epsilon^2 N_{tt} - (N + |E|^2)_{xx} = 0, \tag{3.27b}$$

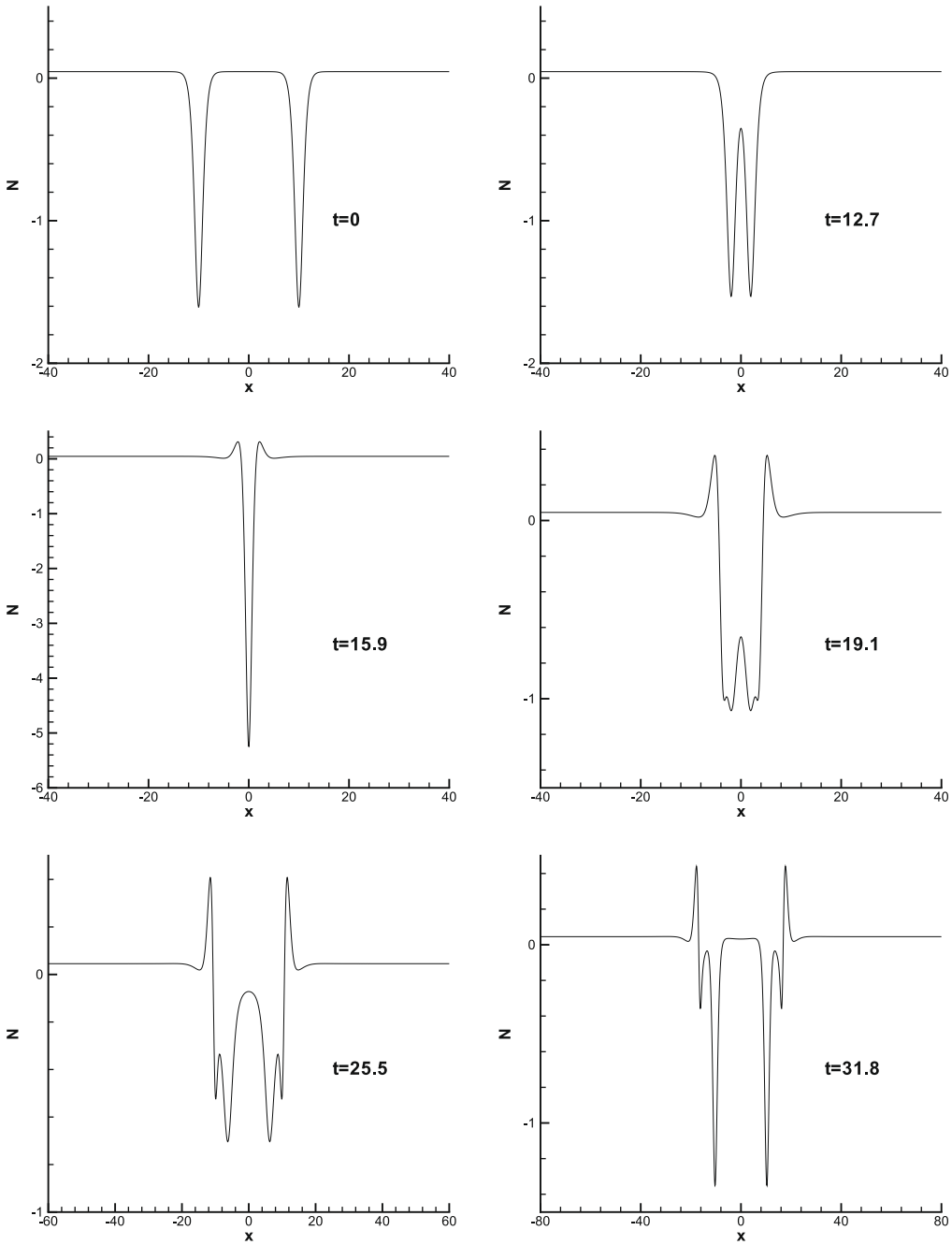

Fig. 3.4. Numerical results at different times in Example 3.3 for case I: ion density N.

with a solitary wave solution given in [14,20,3]

$$E(x,t) = \sqrt{2B^2(1-\epsilon^2C^2)}\,\mathrm{sech}(B(x-Ct))e^{i[(C/2)x-((C/2)^2-B^2)t]}, \tag{3.28}$$

$$N(x,t) = -2B^2\,\mathrm{sech}^2(B(x-Ct)), \tag{3.29}$$

where B, C are constants. The solution decays to zero as $|x| \to \infty$. We compute the problem on the interval $[-32,32]$. First we test the $O(1)$-acoustic speed case, i.e. we choose $\epsilon = 1, B = 1, C = 0.5$ in (3.29). Table 3.1 lists the L^2 and L^∞ errors and orders at $t = 2.0$ with different mesh sizes for the piecewise P^3 and P^4 polynomial bases. Then, we test the subsonic limit case with $\epsilon = 10^{-4}, B = 1$ and $C = 0.5$ in (3.29). Table 3.2 presents the numerical errors and orders at $t = 2.0$ with different mesh sizes

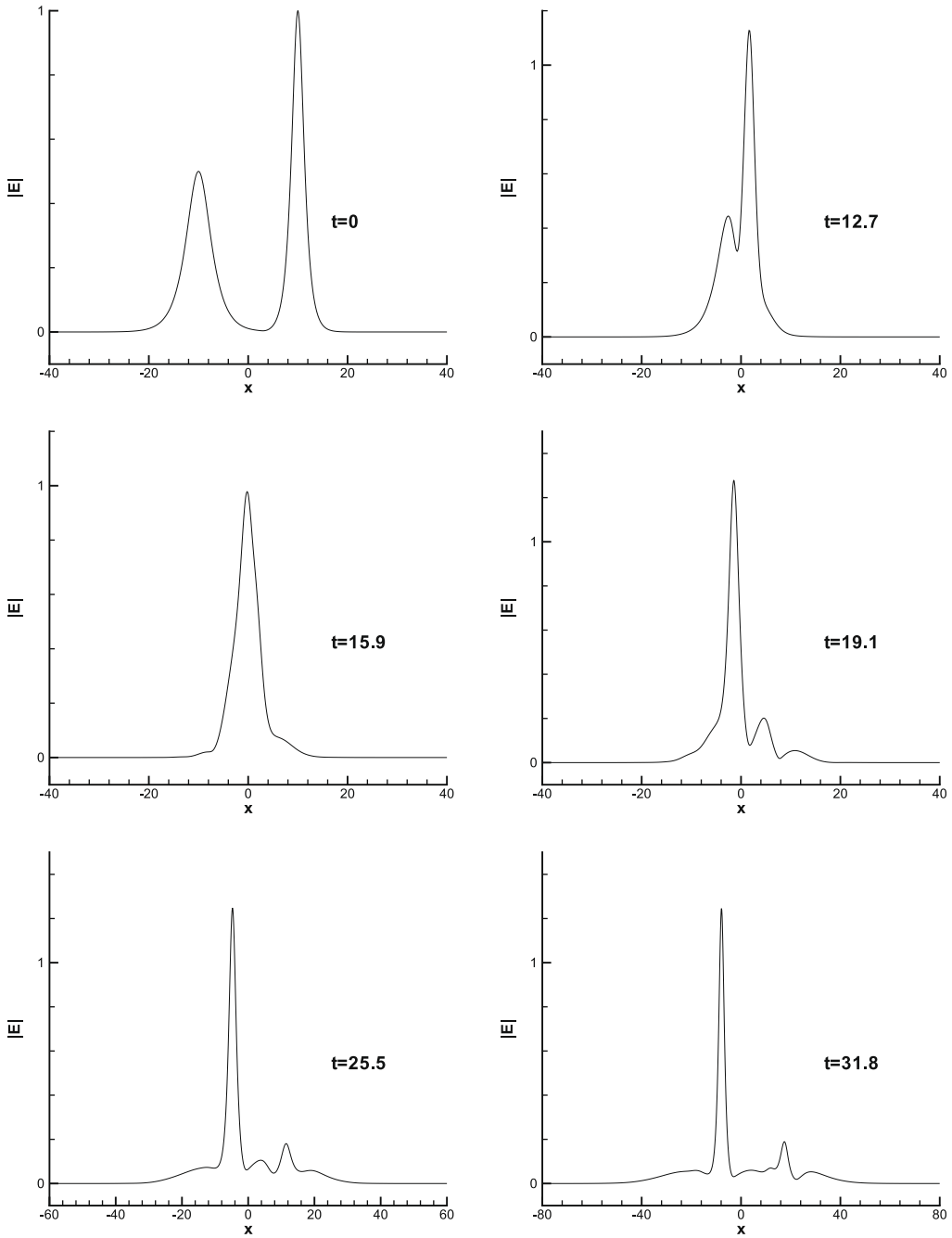

Fig. 3.5. Numerical results at different times in Example 3.3 for case II: electric field $|E|$.

for the piecewise P^3 and P^4 polynomial bases. We can see the convergence order is optimal ($(k+1)$th order for P^k basis) in both cases. In Fig. 3.1, we show the conservation of the conserved quantities D, P and H numerically in both the acoustic speed case and the subsonic case. The results of P^k basis with lower k ($k = 0, 1, 2$) are similar and hence are not shown to save space.

Example 3.2 (*Plane waves*). A family of nonlinear plane-wave solutions to the standard Zakharov system (3.27) can be given in the form [20]

$$E(x,t) = ae^{i(kx-\omega t)}, \tag{3.30}$$

$$N(x,t) = b, \tag{3.31}$$

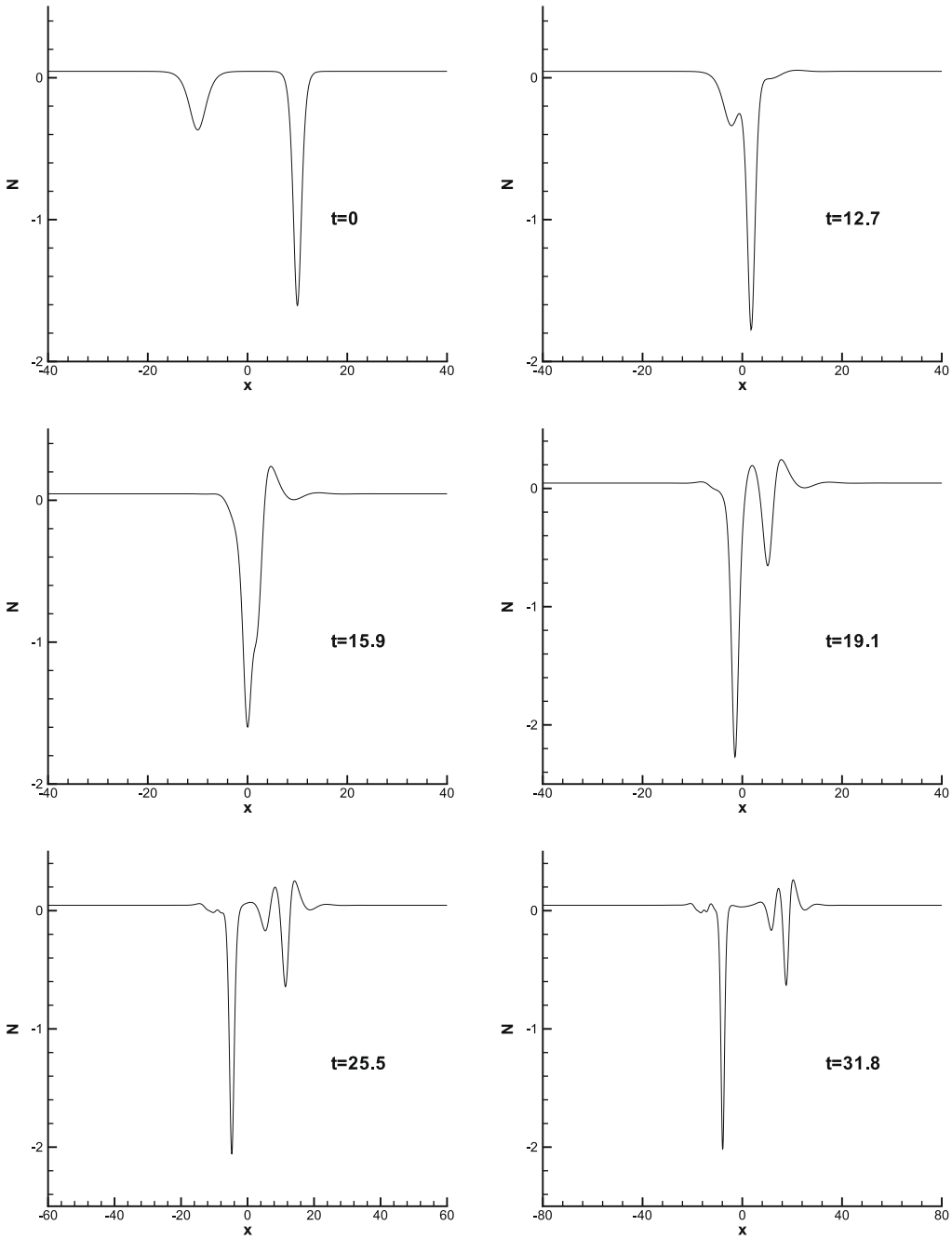

Fig. 3.6. Numerical results at different times in Example 3.3 for case II: ion density N.

provided the dispersion relation $\omega = k^2 + b$ is satisfied. We choose $\epsilon = 1, a = 1, b = 1, k = 7$ and $\omega = 50$. We solve this problem on the interval $[0, 2\pi]$ with piecewise P^4 polynomial basis and mesh size $h = \pi/8$. Fig. 3.2 shows the numerical results at $t = 10$. From Fig. 3.2, we can see that the LDG method provides a good resolution of the nonlinear plane waves and the energies D, P and H are conserved numerically.

Example 3.3 (*Periodic soliton–soliton collisions*). An analytic solution of the standard Zakharov system (3.27) can be found by using the energy method [16]. The solution can be written as

$$E_s(x, t; v, E_{\max}) = \Phi(x - vt)e^{i\varphi(x-ut)}, \tag{3.32}$$

$$N_s(x, t; v, E_{\max}) = \Psi(x - vt), \tag{3.33}$$

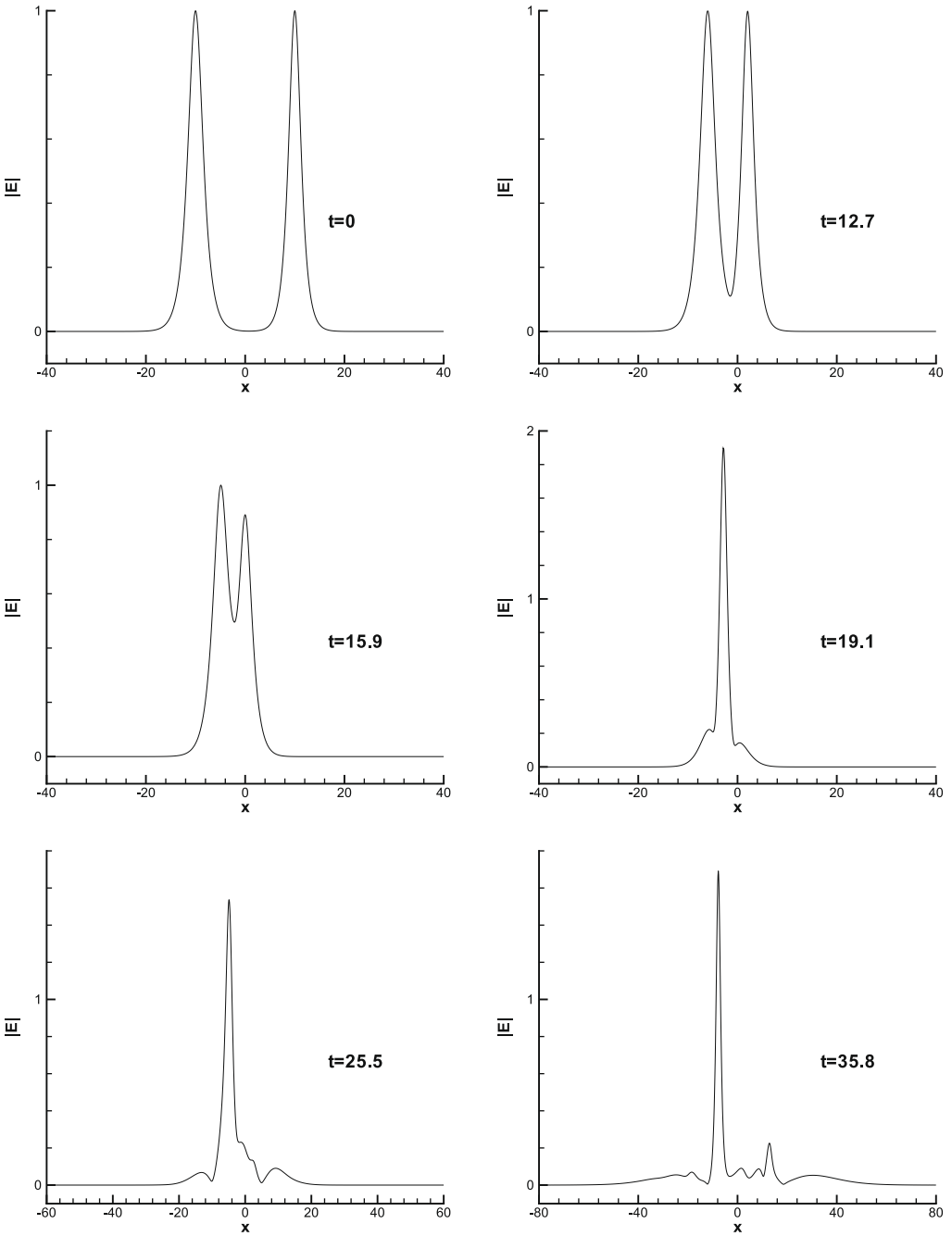

Fig. 3.7. Numerical results at different times in Example 3.3 for case III: electric field $|E|$.

where

$$\Phi(x-vt) = E_{\max}\cdot dn(w,q), \quad \Psi(x-vt) = \frac{|\Phi(x-vt)|^2}{v^2-1} + N_0,$$

$$w = \frac{E_{\max}}{\sqrt{2(1-v^2)}}\cdot(x-vt), \quad q = \frac{\sqrt{E_{\max}^2 - E_{\min}^2}}{E_{\max}},$$

$$\varphi = v/2, \quad \frac{v}{2}L = 2\pi m, \quad m = 1,2,3,\ldots, \; u = \frac{v}{2} + \frac{2N_0}{v} - \frac{E_{\max}^2 + E_{\min}^2}{v(1-v^2)},$$

$$L = \frac{2\sqrt{2(1-v^2)}}{E_{\max}}K(q) = \frac{2\sqrt{2(1-v^2)}}{E_{\max}}K'\left(\frac{E_{\min}}{E_{\max}}\right),$$

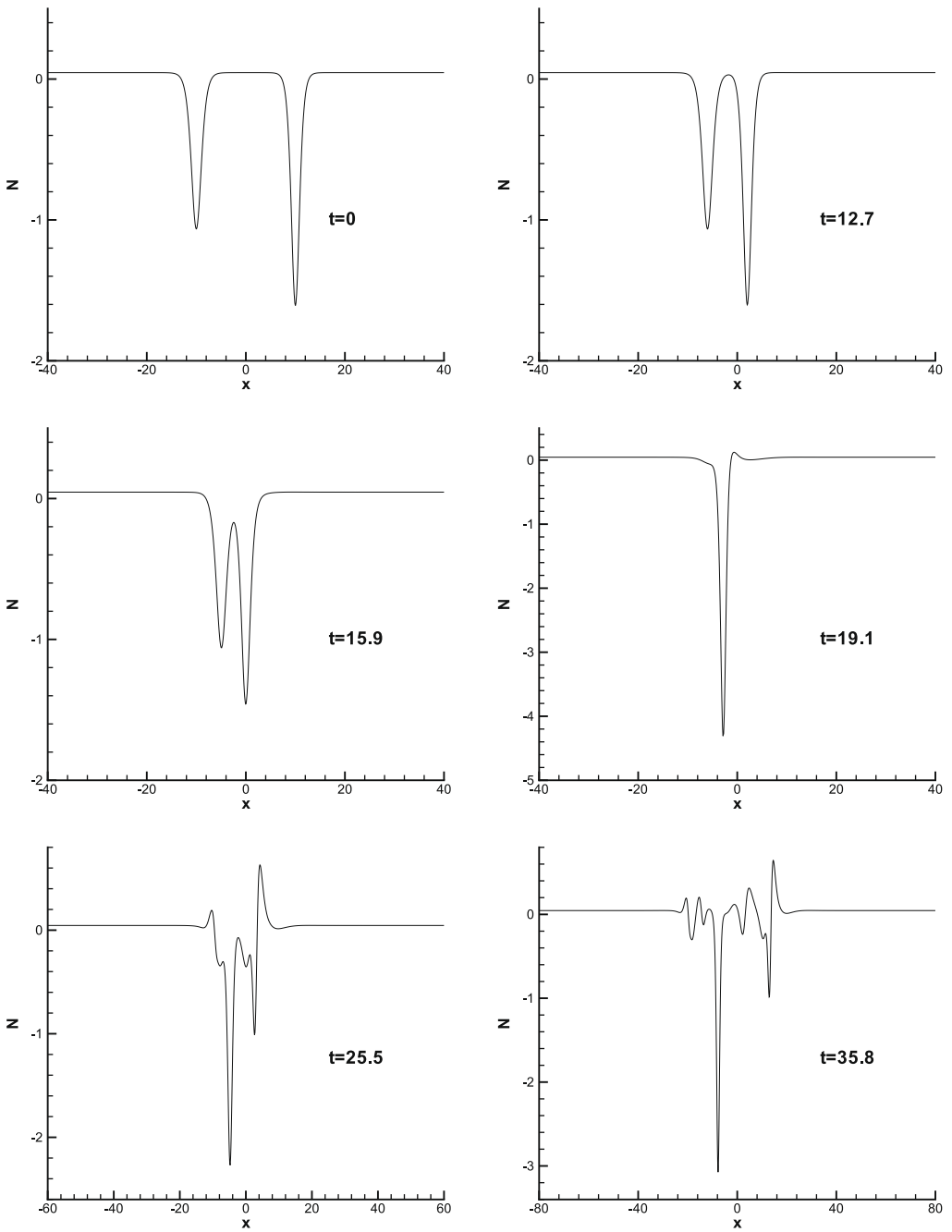

Fig. 3.8. Numerical results at different times in Example 3.3 for case III: ion density *N*.

$dn(w,q)$ is the Jacobian elliptic function, L is the period of the Jacobian elliptic function or the period of the soliton, K and K' are the complete elliptic integrals of the first kind which satisfy $K(q) = K'(\sqrt{1-q^2})$, and N_0 is chosen so that $< N_s >= \frac{1}{L}\int_0^L N_S(x,t)dx = 0$. This solution has been used to test different numerical methods for the Zakharov system in [21,5,12,3].

For easy comparison of the numerical results, we choose the same initial conditions as in [3] to simulate the collision of two solitary waves, which are

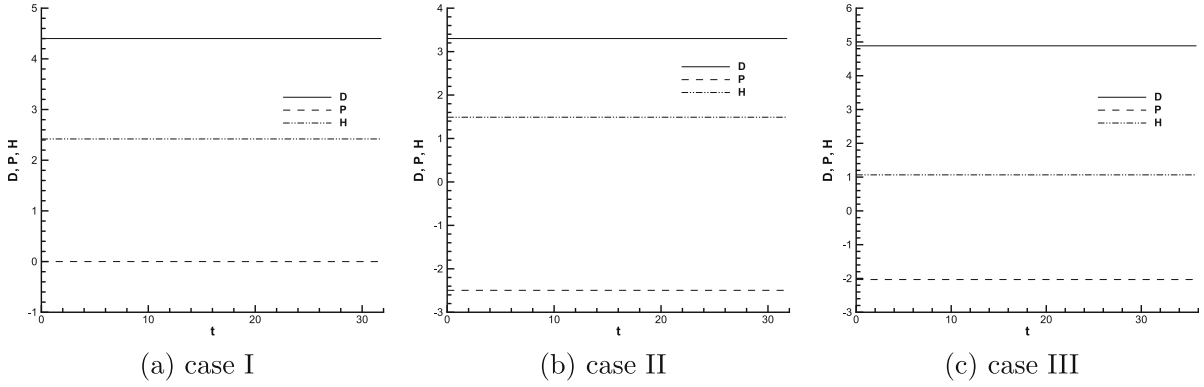

Fig. 3.9. Numerical results in Example 3.3: the energies D, P and H for three cases.

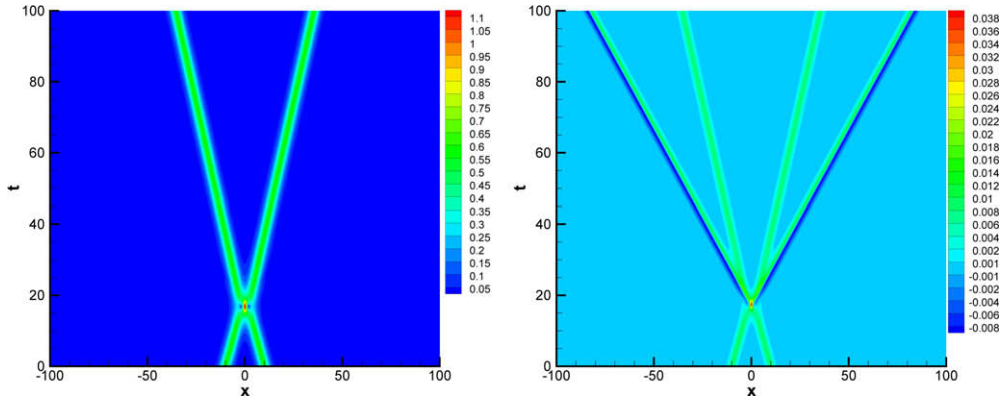

Fig. 3.10. Numerical results in Example 3.4 with $v = 0.5, v/\lambda = 0.02$: $|E|$ (left) and N (right).

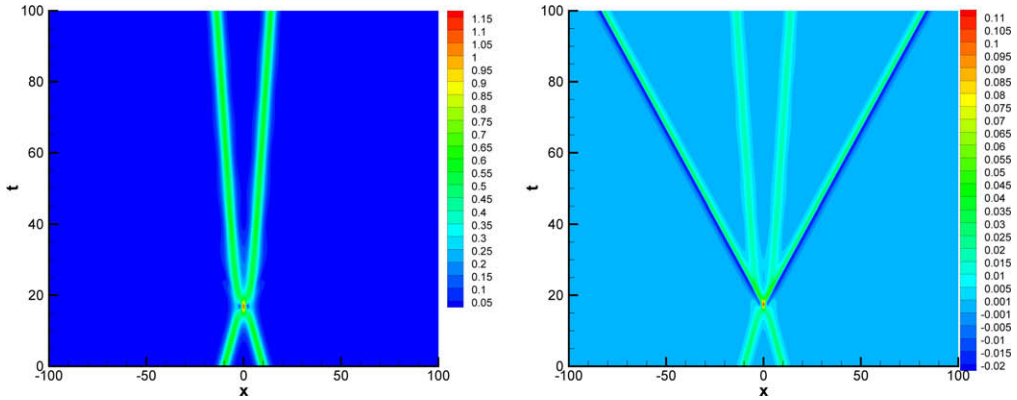

Fig. 3.11. Numerical results in Example 3.4 with $v = 0.5, v/\lambda = 0.06$: $|E|$ (left) and N (right).

$$E(x,0) = E_s(x+p,0,v_1,E^1_{\max}) + E_s(x-p,0,v_2,E^2_{\max}), \tag{3.34}$$
$$N(x,0) = N_s(x+p,0,v_1,E^1_{\max}) + N_s(x-p,0,v_2,E^2_{\max}), \tag{3.35}$$
$$N_t(x,0) = \partial_t N_s(x+p,0,v_1,E^1_{\max}) + \partial_t N_s(x-p,0,v_2,E^2_{\max}), \tag{3.36}$$

where $x = \mp p$ are the initial locations of the two solitons. The parameters are given in Table 3.3.

As in [3], we test the following three cases:

I. Collision of two solitons with equal amplitudes and opposite velocities:

$$E^1_{\max} = E^2_{\max} = 1.0, \quad v_1 = -v_2 = 0.628319, \quad \text{(parameter set A)}.$$

II. Collision of two solitons with different amplitudes and opposite velocities:

$$E^1_{\max} = 0.5, \quad v_1 = 0.628319 \quad \text{(parameter set B)},$$
$$E^2_{\max} = 1.0, \quad v_2 = 0.628319 \quad \text{(parameter set A)}.$$

III. Collision of two solitons with equal amplitudes and opposite velocities but different speeds:

$$E^1_{\max} = 1.0, \quad v_1 = 0.314159 \quad \text{(parameter set C)},$$
$$E^2_{\max} = 1.0, \quad v_2 = -0.628319 \quad \text{(parameter set A)}.$$

In all cases, we take $p = 10$. We solve the problem in the interval $[-80,80]$ with piecewise P^3 polynomial basis and mesh size $h = 1/2$. Figs. 3.3–3.8 show the profiles of $|E|$ and N at different time for each case. It is known that the standard Zakharov system is not integrable. This implies that collision between solitons cannot be absolutely elastic. In case I, Fig. 3.3 shows the collision of two solitons with equal amplitudes and opposite velocities reduces the maximum $E_{\max}$ of both waves. Comparing

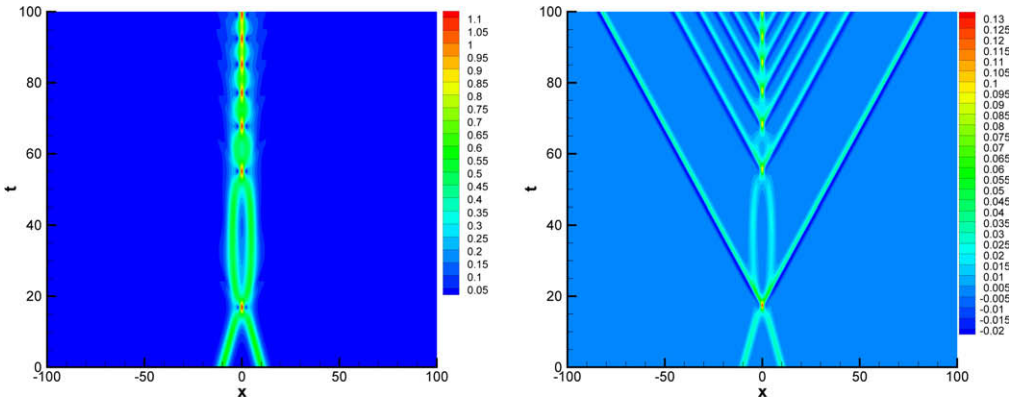

Fig. 3.12. Numerical results in Example 3.4 with $v = 0.5, v/\lambda = 0.07$: $|E|$ (left) and N (right).

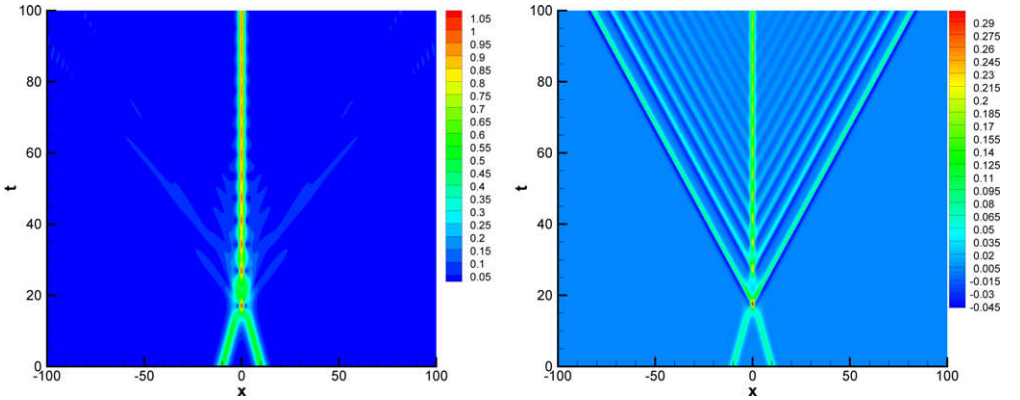

Fig. 3.13. Numerical results in Example 3.4 with $v = 0.5, v/\lambda = 0.2$: $|E|$ (left) and N (right).

with the same simulations performed in [21,5,12,3], the LDG scheme shows good resolution. In case II, from Fig. 3.5 we can observe the soliton with larger peak value absorbs some waves during the collision. After collision, the soliton with a larger peak value $E^1_{\max}$ becomes bigger than its value before the collision, and the soliton with smaller peak value $E^2_{\max}$ becomes smaller. In case III, from Fig. 3.7 we can see that the soliton with larger speed will absorb some waves during the collision. The numerical results of each case compare well with the simulation results by Bao et al. [3].

Three conservation laws D, P and H are known to the standard Zakharov system. Two of them (D and H) have been proved for the LDG scheme. In Fig. 3.9, it shows that these energies are conserved well numerically by the LDG scheme.

Example 3.4 (*Soliton–soliton collisions*). Consider the one-dimensional generalized Zakharov system

$$iE_t + E_{xx} + 2NE + 2\lambda|E|^2E = 0, \tag{3.37}$$

$$\epsilon^2 N_{tt} - (N - v|E|^2)_{xx} = 0, \tag{3.38}$$

with a family of one-soliton solutions [14],

$$E_s(x,t;\eta,v) = \left[\lambda + \frac{v}{\epsilon^2}(1/\epsilon^2 - v^2)^{-1}\right]^{-\frac{1}{2}} U_s, \tag{3.39a}$$

$$U_s = 2i\eta\,\mathrm{sech}[2\eta(x - vt)]\exp[ivx/2 + i(4\eta^2 - v^2/4)t + i\Phi_0], \tag{3.39b}$$

$$N_s(x,t;\eta,v) = \frac{v}{\epsilon^2}(1/\epsilon^2 - v^2)^{-1}|E_s|^2, \tag{3.39c}$$

where η, v are the soliton's amplitude and velocity, and Φ_0 is a trivial phase constant. With $\lambda > 0$ and $v > 0$, the solitons exist in two different regions: the subsonic region

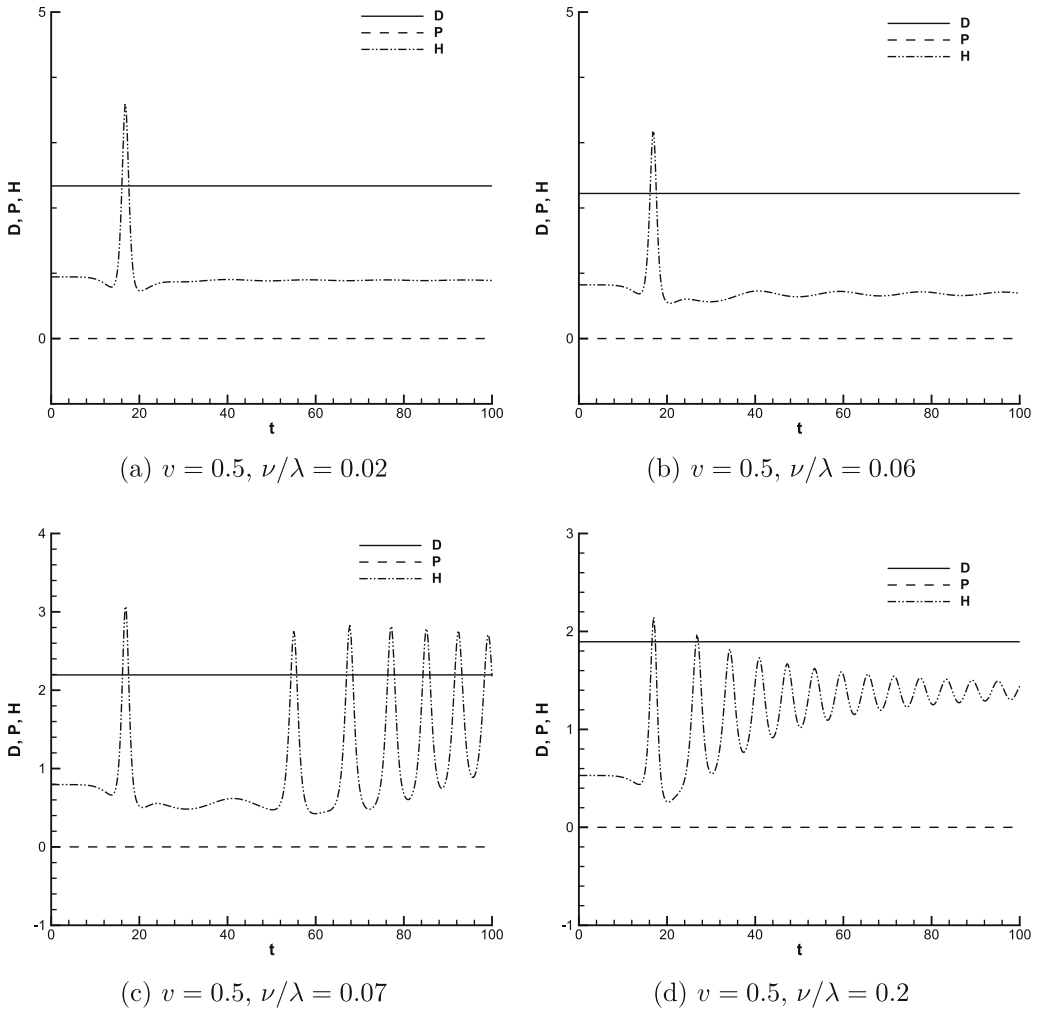

Fig. 3.14. Numerical results in Example 3.4: the energies D, P and H.

$$v^2 < \frac{1}{\epsilon^2}, \tag{3.40}$$

and the transonic (or supersonic) region

$$v^2 > \frac{1}{\epsilon^2}(1 + \nu/\lambda). \tag{3.41}$$

For simplicity, we consider the symmetric collisions, where the two solitons have the same speed and same amplitude but propagate in the opposite directions.

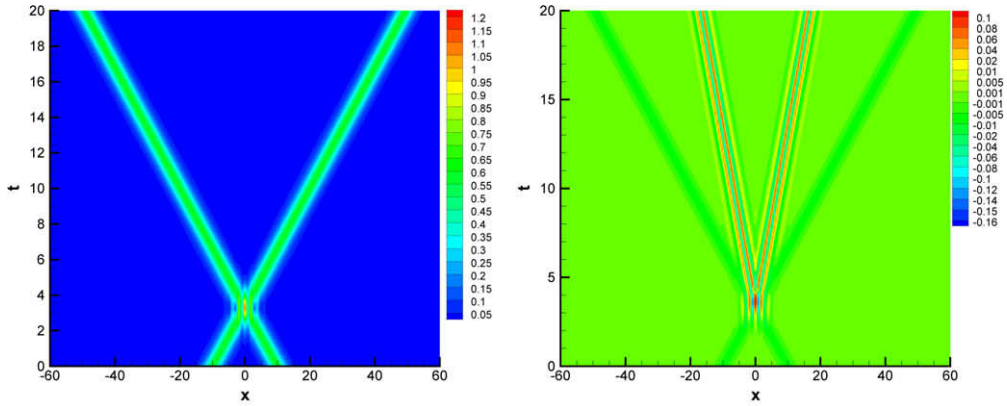

(a) $v = 3,\ \nu/\lambda = 0.2$

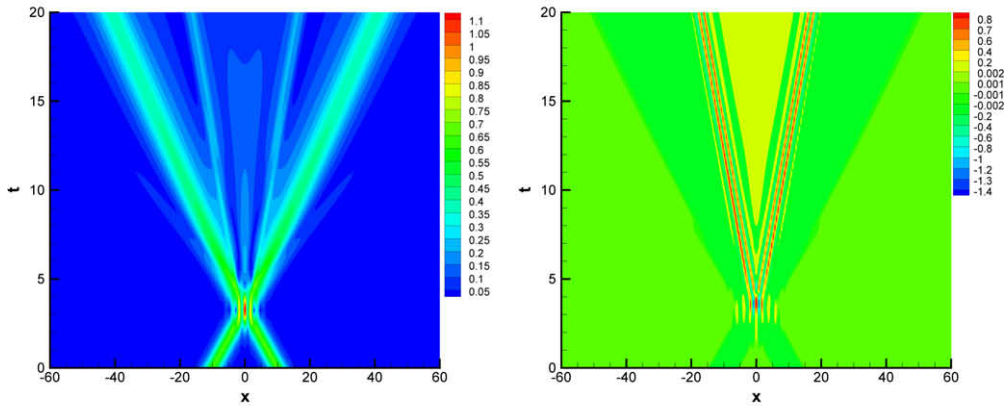

(b) $v = 3,\ \nu/\lambda = 1.45$

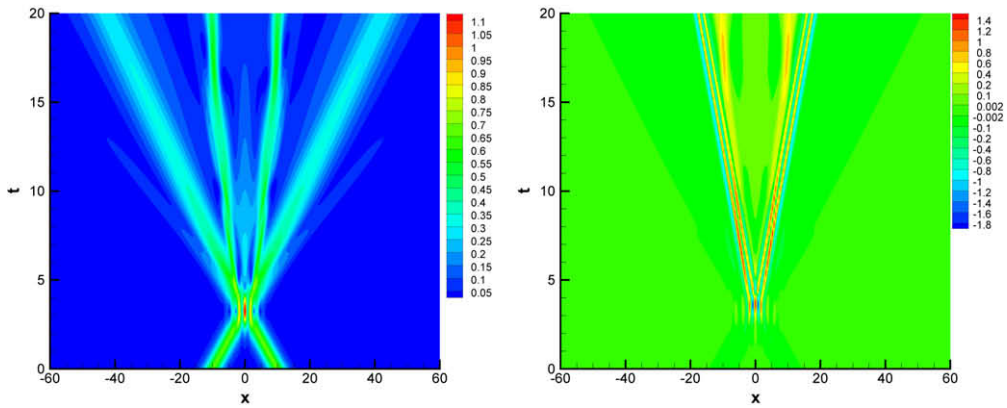

(c) $v = 3,\ \nu/\lambda = 1.75$

Fig. 3.15. Numerical results in Example 3.4: $|E|$ (left) and N (right).

Table 3.4
Accuracy test in Example 3.5 for the plane-wave solution at time $t = 1$, with piecewise P^3 and P^4 polynomial bases on $m \times m$ uniform meshes.

	m	P^3				P^4			
		L^∞ error	Order	L^2 error	Order	L^∞ error	Order	L^2 error	Order
$Re(E)$	4	1.26E−01	–	1.07E−01	–	1.17E−02	–	1.29E−02	–
	8	8.10E−03	3.96	7.11E−03	3.91	6.16E−04	4.25	4.99E−04	4.69
	16	3.41E−04	4.57	3.50E−04	4.35	1.90E−05	5.02	1.45E−05	5.11
	32	3.35E−05	3.35	2.59E−05	3.76	6.44E−07	4.88	4.70E−07	4.94
	64	1.21E−06	4.79	1.00E−06	4.69	1.15E−08	5.81	1.06E−08	5.47
$Im(E)$	4	1.26E−01	–	1.07E−01	–	1.17E−02	–	1.29E−02	–
	8	8.10E−03	3.96	7.11E−03	3.91	6.16E−04	4.25	4.99E−04	4.69
	16	3.41E−04	4.57	3.50E−04	4.35	1.90E−05	5.02	1.45E−05	5.11
	32	3.35E−05	3.35	2.59E−05	3.76	6.44E−07	4.88	4.70E−07	4.94
	64	1.21E−06	4.79	1.00E−06	4.69	1.15E−08	5.81	1.06E−08	5.47
N	4	5.31E−02	–	1.58E−01	–	3.51E−02	–	3.71E−02	–
	8	9.91E−03	2.42	1.42E−02	3.48	1.20E−04	8.17	2.33E−04	7.31
	16	3.05E−04	5.02	3.94E−04	5.17	3.82E−06	4.98	6.13E−06	5.25
	32	3.97E−05	2.94	6.02E−05	2.71	7.12E−08	5.75	9.15E−08	6.07
	64	1.41E−06	4.81	2.20E−06	4.77	2.05E−09	5.12	2.22E−09	5.37

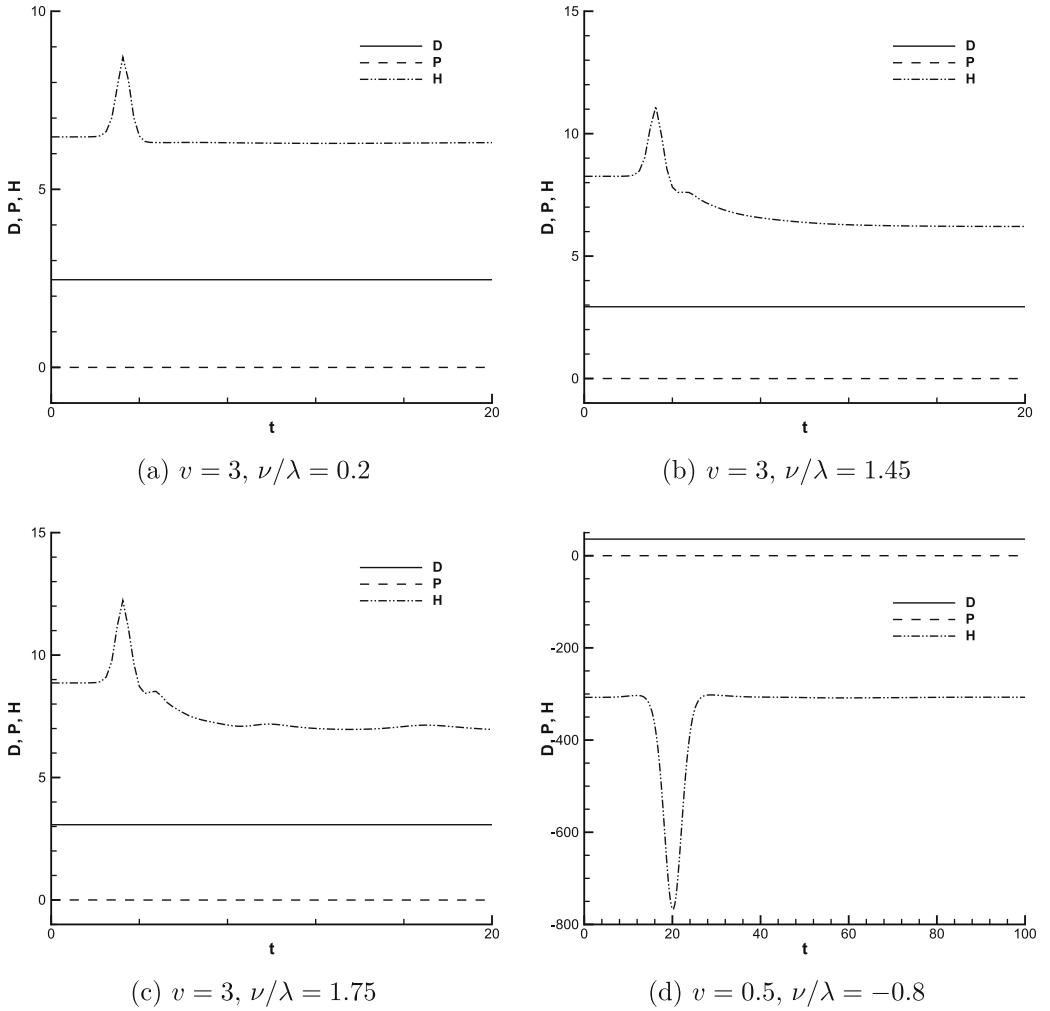

Fig. 3.16. Numerical results in Example 3.4: the energies D, P and H .

$$E(x,0) = E_s(x+p,0,\eta,v) + E_s(x-p,0,\eta,-v),$$
$$N(x,0) = N_s(x+p,0,\eta,v) + N_s(x-p,0,\eta,-v).$$

We set $\epsilon = 1, \Phi_0 = 0, p = 10$ and $\eta = 0.3$ in the following. All computations are performed with piecewise P^3 polynomial basis with mesh size $h = 1$ in the interval $[-128, 128]$. We define the energy H

$$H = \int_\Omega \left(|\nabla E|^2 + \frac{1}{2}(\boldsymbol{V} \cdot \boldsymbol{V} + N^2) - 2N|E|^2 + \lambda |E|^4 \right) d\boldsymbol{x}.$$

However, H is not conserved when $v \neq 2$.

First we consider the collisions of two solitons with subsonic propagation speeds $v = 0.5, \lambda = 1$ and $v = 0.02$ (Fig. 3.10), 0.06 (Fig. 3.11), 0.07 (Fig. 3.12) and 0.2 (Fig. 3.13), respectively. It is known that the generalized Zakharov system is close to the cubically nonlinear Schrödinger equation when v/λ is sufficiently small. This means that the collisions between solitons are nearly elastic. After the collisions, two solitons $|E|$ propagate in their original directions but with smaller speeds (Fig. 3.10) and the non-dispersive waves N generate a pair of non-dispersive waves. With the increase of v/λ, the solitons' speed becomes smaller (Fig. 3.11) and a series of non-dispersive waves are emitted after the collision point. In Fig. 3.14, from (a) and (b) we can see the energies D and P are conserved, and H increases significantly when the collision of two solitons takes place, and becomes smaller than its value before the collisions afterwards. When v/λ is larger than a critical value (Figs. 3.12 and 3.13), the solitons are not generated again after the collision and a series of stronger non-dispersive waves are emitted. As shown in [17], the critical value is strongly dependent on the soliton speed v. When the system is far from being exactly integrable, the collision results in a fusion of the solitons into a new soliton like state. In Fig. 3.14, from (c) and (d), we find the energies D and P are still conserved. H increases when the collision happens. From the oscillation of H after the first collision, the fusion can be viewed as a series of collisions where two solitons become closer and closer.

Next we consider the collisions of two solitons in the supersonic region with $v = 3, \lambda = 1$ and $v = 0.2, 1.45$ and 1.75 (Fig. 3.15), respectively. We can see that, when v/λ is small, the collision seems to be elastic and the solitons' speeds after the collision are almost the same as before the collision. In (b) and (c) of Fig. 3.15, when v/λ becomes larger, a pair of solitons

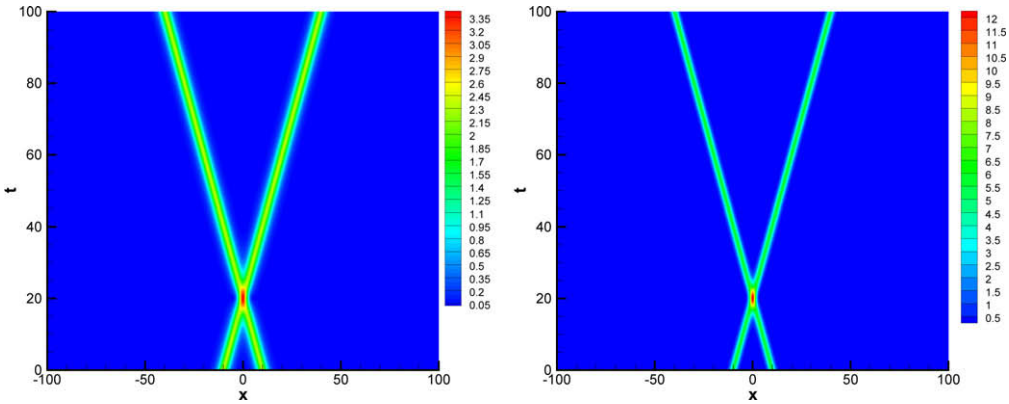

Fig. 3.17. Numerical results in Example 3.4 with $v = 0.5, v/\lambda = -0.8$: $|E|$ (left) and N (right).

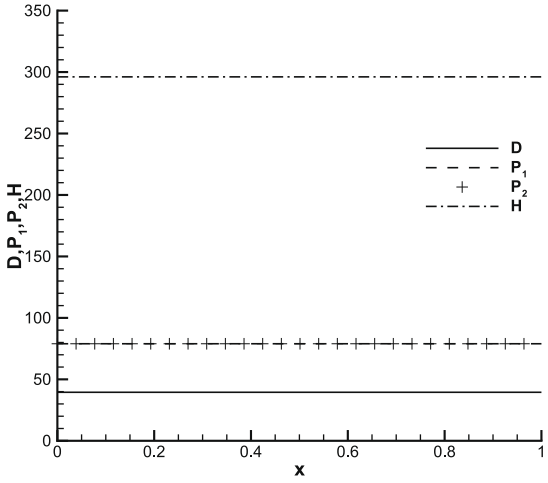

Fig. 3.18. Numerical results in Example 3.5: the energies D, $\boldsymbol{P}$ and H.

with slower speed is emitted after the collision. As observed in [17], it also can be found that the amplitudes of these slower solitons increase with the growth of v/λ. The increasing of v/λ also gives rise to radiative losses. In Fig. 3.16(a)–(c), we find the energies D and P are conserved and H grows when the collision happens. After the collision, the energy H becomes smaller than its value before the collision.

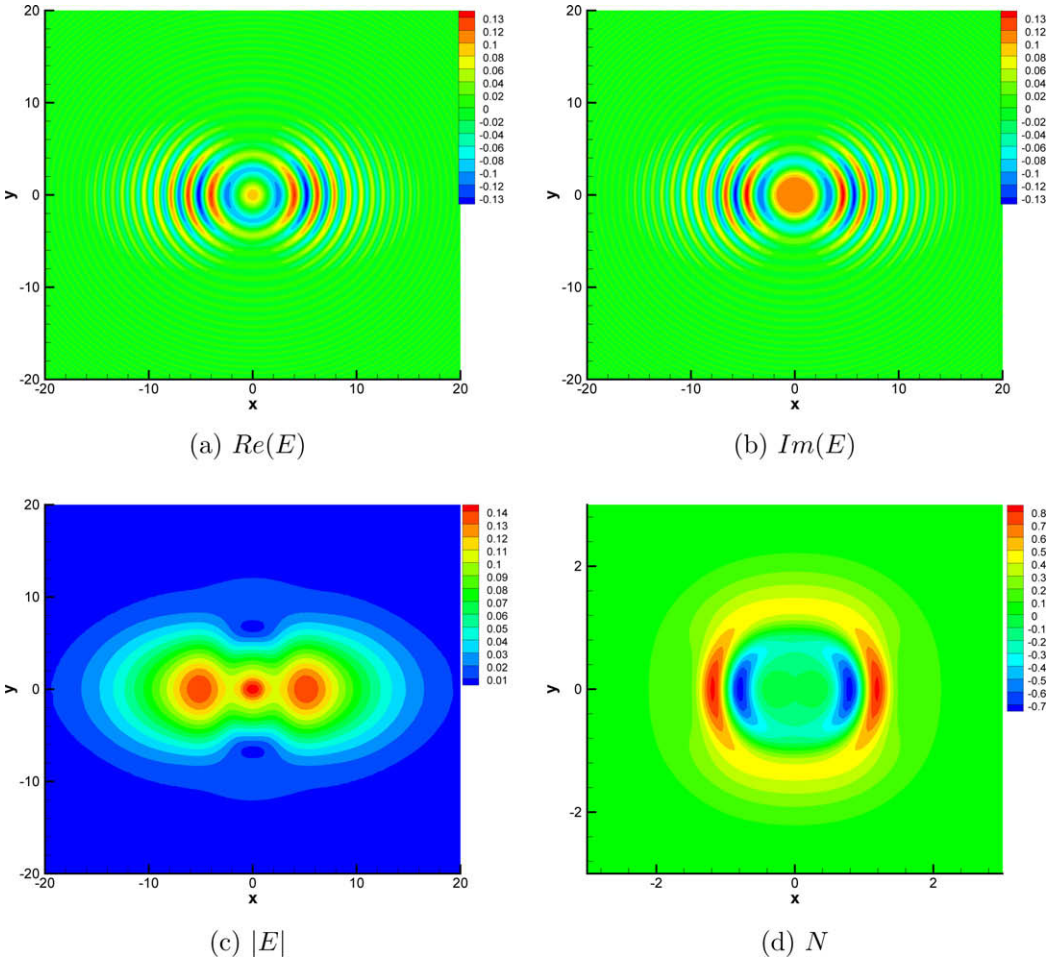

Fig. 3.19. Numerical results in Example 3.6 with piecewise P^4 polynomial basis and mesh size $h = 1/2$ at time $t = 1$: (a) $Re(E)$, (b) $Im(E)$, (c) $|E|$, and (d) N.

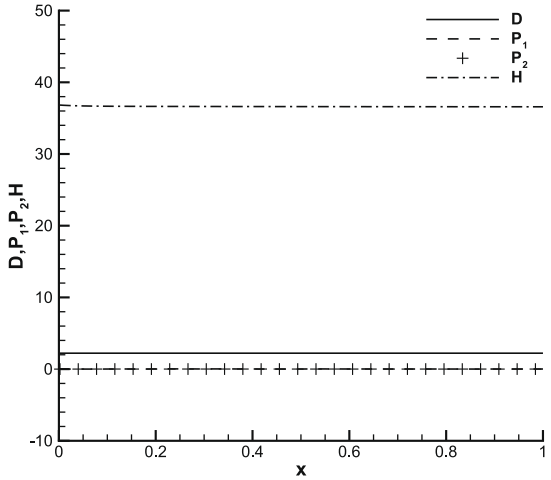

Fig. 3.20. Numerical results in Example 3.6: the energies D, $\boldsymbol{P}$ and H.

Finally, we consider the case with $\lambda < 0$. We set $v = 0.5, \lambda = -1$ and $v = 0.8$, which falls in the subsonic region. Fig. 3.17 shows that the collision seems elastic and no significant radiation is observed. Fig. 3.16(d) shows the energies D and P are conserved and H after the collision is almost the same as its value before collision.

Our numerical results of the collisions of the generalized Zakharov system are very well consistent with the simulations performed in [17].

3.2. The two-dimensional Zakharov system

Example 3.5 (*The two-dimensional plane waves*). We use this example to test the accuracy of the LDG scheme in 2D. Nonlinear plane-wave solutions to the 2D standard Zakharov system (2.7a) and (2.7b) can be given in the form

$$E(x,t) = ae^{i(k_1x+k_2y-\omega t)}, \tag{3.42}$$

$$N(x,t) = b, \tag{3.43}$$

provided the dispersion relation $\omega = k_1^2 + k_2^2 + b$ is satisfied. We choose $\epsilon = 1, a = 1, b = 1, k_1 = 1, k_2 = 1$ and $\omega = 3$. We solve this problem on the domain $[0, 2\pi] \times [0, 2\pi]$ with piecewise P^3 and P^4 polynomial bases and $m \times m$ uniform meshes. In Table 3.4, we can see the order of convergence is optimal. Though we do not list the P^0, P^1, P^2 cases to save space, optimal convergence orders are also observed in these numerical tests. Fig. 3.18 shows that the energies D, P and H are conserved under piecewise P^4 polynomial basis on a 16×16 uniform mesh.

Example 3.6 (*The two-dimensional standard Zakharov system*). To show the capability of the LDG scheme, we consider the two-dimensional standard Zakharov system

$$iE_t + \Delta E - NE = 0,$$

$$\epsilon^2 N_{tt} - \Delta(N + |E|^2) = 0,$$

with the initial condition

$$E(x,y,0) = \frac{2}{e^{x^2+y^2} + e^{-(x^2+y^2)}} e^{i5/\cosh\left(\sqrt{4x^2+y^2}\right)},$$

$$N(x,y,0) = e^{-(x^2+y^2)}, \quad N_t(x,y,0) = 0.$$

This example is taken from [3] with $\epsilon = 1$. We solve the problem on the rectangle $[-64, 64] \times [-64, 64]$ with mesh size $h = 1/2$ by using piecewise P^4 polynomial basis. Fig. 3.19 shows the $Re(E), Im(E), |E|$ and N at time $t = 1$. Fig. 3.20 shows the energies D, P and H are conserved numerically. The numerical results compare very well with the results presented in [3].

4. Conclusion

In this paper, we have constructed a LDG method for the generalized Zakharov system. We prove that the LDG method conserves the wave energy D of the generalized Zakharov system and the Hamiltonian H if the generalized Zakharov system has this conserved quantity. Numerical tests have been performed to show the numerical optimal accuracy. Some applications, such as plane waves, soliton–soliton collisions of the standard and generalized Zakharov system and a two-dimensional standard Zakharov system, have also been simulated to show the capability of the LDG method for the Zakharov system.

References

[1] F. Bassi, S. Rebay, A high-order accurate discontinuous finite element method for the numerical solution of the compressible Navier–Stokes equations, J. Comput. Phys. 131 (1997) 267–279.
[2] W. Bao, F. Sun, Efficient and stable numerical methods for the generalized and vector Zakharov system, SIAM J. Sci. Comput. 26 (2005) 1057–1088.
[3] W. Bao, F. Sun, G.W. Wei, Numerical methods for the generalized Zakharov system, J. Comput. Phys. 190 (2003) 201–228.
[4] Q. Chang, B. Guo, H. Jiang, Finite difference method for generalized Zakharov system, Math. Comput. 64 (1995) 537–553.
[5] Q. Chang, H. Jiang, A conservative difference scheme for the Zakharov system, J. Comput. Phys. 113 (1994) 309–319.
[6] B. Cockburn, S. Hou, C.-W. Shu, The Runge–Kutta local projection discontinuous Galerkin finite element method for conservation laws IV: the multidimensional case, Math. Comput. 54 (1990) 545–581.
[7] B. Cockburn, S.-Y. Lin, C.-W. Shu, TVB Runge–Kutta local projection discontinuous Galerkin finite element method for conservation laws III: one-dimensional systems, J. Comput. Phys. 84 (1989) 90–113.
[8] B. Cockburn, C.-W. Shu, TVB Runge–Kutta local projection discontinuous Galerkin finite element method for conservation laws II: general framework, Math. Comput. 52 (1989) 411–435.
[9] B. Cockburn, C.-W. Shu, The Runge–Kutta discontinuous Galerkin method for conservation laws V: multidimensional systems, J. Comput. Phys. 141 (1998) 199–224.
[10] B. Cockburn, C.-W. Shu, The local discontinuous Galerkin method for time-dependent convection–diffusion systems, SIAM J. Numer. Anal. 35 (1998) 2440–2463.
[11] J. Gibbons, S.G. Thornhill, M.J. Wardrop, D. Ter Haar, On the theory of Langmuir solitons, J. Plasma Phys. 17 (1977) 153–170.
[12] R. Glassey, Approximate solutions to the Zakharov system via finite difference, J. Comput. Phys. 100 (1992) 377–383.
[13] R. Glassey, Convergence of an energy-preserving scheme for the Zakharov equations in one space dimension, Math. Comput. 58 (1992) 83–102.
[14] H. Hadouaj, B.A. Malomed, G.A. Maugin, Soliton–soliton collisions in a generalized Zakharov system, Phys. Rev. A 44 (1991) 3932–3940.

[15] H. Hadouaj, B.A. Malomed, G.A. Maugin, Dynamics of a soliton in a generalized Zakharov system with dissipation, Phys. Rev. A 44 (1991) 3925–3931.
[16] P.J. Hansen, D.R. Nicholson, Simple soliton solutions, Am. J. Phys. 47 (1979) 769–771.
[17] S. Jin, P.A. Markowich, C. Zheng, Numerical simulation of a generalized Zakharov system, J. Comput. Phys. 201 (2004) 376–395.
[18] S. Jin, C. Zheng, A time-splitting spectral method for the generalized Zakharov system in multi-dimensions, J. Sci. Comput. 26 (2006) 127–149.
[19] D. Levy, C.-W. Shu, J. Yan, Local discontinuous Galerkin methods for nonlinear dispersive equations, J. Comput. Phys. 196 (2004) 751–772.
[20] P.K. Newton, Wave interactions in the singular Zakharov system, J. Math. Phys. 32 (1991) 431–440.
[21] G.L. Payne, D.R. Nicholson, R.M. Downie, Numerical solution of the Zakharov equations, J. Comput. Phys. 50 (1983) 482–498.
[22] W.H. Reed, T.R. Hill, Triangular mesh method for the neutron transport equation, Technical Report LA-UR-73-479, Los Alamos Scientific Laboratory, Los Alamos, NM, 1973.
[23] C.-W. Shu, S. Osher, Efficient implementation of essentially non-oscillatory shock-capturing schemes, J. Comput. Phys. 77 (1988) 439–471.
[24] Y. Xia, Y. Xu, C.-W. Shu, Efficient time discretization for local discontinuous Galerkin methods, Discr. Contin. Dyn. Syst. Ser. B 8 (2007) 677–693.
[25] Y. Xia, Y. Xu, C.-W. Shu, Local discontinuous Galerkin methods for the Cahn–Hilliard type equations, J. Comput. Phys. 227 (2007) 472–491.
[26] Y. Xia, Y. Xu, C.-W. Shu, Application of the local discontinuous Galerkin method for the Allen–Cahn/Cahn–Hilliard system, Commun. Comput. Phys. 5 (2009) 821–835.
[27] Y. Xu, C.-W. Shu, Local discontinuous Galerkin methods for three classes of nonlinear wave equations, J. Comput. Math. 22 (2004) 250–274.
[28] Y. Xu, C.-W. Shu, Local discontinuous Galerkin methods for nonlinear Schrödinger equations, J. Comput. Phys. 205 (2005) 72–97.
[29] Y. Xu, C.-W. Shu, Local discontinuous Galerkin methods for two classes of two-dimensional nonlinear wave equations, Physica D 208 (2005) 21–58.
[30] Y. Xu, C.-W. Shu, Local discontinuous Galerkin methods for the Kuramoto–Sivashinsky equations and the Ito-type coupled KdV equations, Comput. Meth. Appl. Mech. Eng. 195 (2006) 3430–3447.
[31] Y. Xu, C.-W. Shu, A local discontinuous Galerkin method for the Camassa–Holm equation, SIAM J. Numer. Anal. 46 (2008) 1998–2021.
[32] J. Yan, C.-W. Shu, A local discontinuous Galerkin method for KdV type equations, SIAM J. Numer. Anal. 40 (2002) 769–791.
[33] J. Yan, C.-W. Shu, Local discontinuous Galerkin methods for partial differential equations with higher order derivatives, J. Sci. Comput. 17 (2002) 27–47.
[34] V.E. Zakharov, Collapse of Langmuir waves, Sov. Phys. JETP 35 (1972) 908–914.
[35] Q. Zhang, Z. Wu, Numerical simulation for porous medium equation by local discontinuous Galerkin finite element method, J. Sci. Comput. 38 (2009) 127–148.